Mathematical Modeling of Oceanic Phytoplankton Blooms in Chaotic Flows

Mara Freilich

Advisors: Baylor Fox-Kemper and Bjorn Sandstede

A thesis submitted in partial fulfillment of the requirements for the degree of Bachelor of Science with Honors in Applied Math

Abstract

Phytoplankton blooms are geochemically and ecologically important, but current understanding of the causes of phytoplankton blooms provides little power to predict the timing, extent, and distribution of blooms. In this thesis, I discuss the implications of light limitation for phytoplankton bloom patchiness and community structure by modeling phytoplankton as reacting tracers in a reaction-advection-diffusion system. I use non-dimensional parameters to develop general principles of bloom dynamics with light limitation that can be tested against empirical results. I first develop an exact Lagrangian model of advection and diffusion with no-flux boundaries to represent a vertical water column and compare the properties of tracers in that model to known properties of a tracer in a turbulent mixed layer. I then use both numerical simulations and exact solutions to systematically build towards understanding the individual interactions between reaction, advection, and diffusion in a reaction-advection-diffusion system with non-linear source terms. I find that spatially variable forcing is required to develop patchiness in a reaction-advection-diffusion system. I also analyze the emergence of temporal heterogeneity in bulk phytoplankton concentrations when the ratio of physical and biological timescales is $\sim \mathcal{O}(1)$ and conclude that non-steady equilibria are due to the degree of spatial heterogeneity as well as to advection and diffusion rates. Finally, I demonstrate one possible mechanism for an interaction between light limitation, turbulence, and predator-prey dynamics.

Contents

1 Background

Phytoplankton account for the majority of marine productivity, are a significant carbon sink, and a crucial energy resource for marine animals. Major plankton blooms, such as the spring bloom in the North Atlantic are known to sequester large amounts of carbon in the oceans. The magnitude and dynamics of plankton blooms are dependent on environmental conditions such as nutrients, light, temperature, turbulence, and other plankton species. In particular, plankton distribution has been observed to be spatially variable and this patchiness has been attributed to a number of factors including both biological processes (birth, death, predation) and physical mixing [26].

Growing phytoplankton populations can be understood as similar to reactive chemicals. When the concentration of a population grows or decays through time as it is being moved by a turbulent fluid the population is called a reacting tracer. Mathematical tools have proven useful for understanding the dynamics of reacting tracers, both chemical and biological, in chaotic fluids. This project touches on a number of topics from non-linear dynamics, including bifurcation of steady states, with the ratio between biological reaction rate and stirring rate functioning as a bifurcation parameter, and coupled oscillators. Previous studies investigated the role of both advection and diffusion separately in determining the role of fluid dynamics in generating phytoplankton dynamics. Theoretical [6] and numerical approaches [8, 19, 23, 29, 34, 37] have been used.

The theoretical approach used by Bennett and Denman, which involved dimensional analysis and relied on analyzing variance spectra, found that in mesoscale eddies, spatial variability of a nutrient, whether that nutrient is advected or not is sufficient to generate patchiness when using a three dimensional (nutrients, phytoplankton, zooplankton) non-linear model for biological dynamics [6]. Subsequent work specifically on generation of phytoplankton patchiness due to turbulent stirring has largely focused on using numerical simulations to determine what aspects of theoretical fluid dynamics or biological dynamics are necessary to generate realistic patchiness in a model. Investigation of the role of advection (rather than diffusion) led to the insight that the relative rate of biological reactions to stirring processes can be one controlling factor in generating the spatial patterns of zooplankton and phytoplankton [1]. More complex numerical studies have found that topographical features such as islands can cause increased primary productivity by generating vortices that increase the residence time of phytoplankton in high nutrient areas [34].

Chaotic advection can give rise to new phenomena in chemical reaction systems. In a flame combustion system, chaotic stirring leads to quenching of the reaction. The quenching occurs at a saddle node bifurcation [28]. The behavior near the bifurcation depends, as in biological systems, on the ratio between reaction rate and stirring rate, called the Damkohler number in chemical systems [37]. The rate of progress towards completion of a reaction can also depend on the characteristics of fluid motion. Tsang (2009) found that for a bimolecular irreversible chemical reaction, products decayed exponentially, with the rate scaling with the Lyapunov exponent of the fluid, until nearing completion, when the system follows algebraic chemical kinetic rate laws [38].

Tsang (2009) was also able to apply the theory of passive scalars to understanding the system by investigating the limits of large and small Damkohler numbers.

Physical forcing is commonly invoked to explain the rapid accumulation of biomass that characterizes phytoplankton blooms, but a number of different mechanisms for the influence of turbulence on bloom formation have been proposed. Mathematical modeling is a useful tool for translating theoretical models of bloom formation into testable predictions [16, 20, 25, 36].

Traditionally, the mixed layer depth, the depth of the ocean surface layer that is characterized by vertically homogenous density, was thought to control bloom dynamics through its effect on light exposure. Sverdrup hypothesized in what is known as the "critical depth hypothesis" that bloom onset occurs when the upper ocean warms and stratifies such that the thermocline is at a critical depth, defined as the depth at which net production of plankton, integrated over the whole mixed layer is equal to net loss, integrated over the whole mixed layer [35]. Production is thought to vary with depth, since light availability is reduced deeper in the water column, while loss is assumed to be constant with depth. This hypothesis assumes that plankton are uniformly distributed through the mixed layer and that active mixing occurs in the entire mixed layer such that phytoplankton are exposed to all light levels in the water column. Subsequent work suggested that not only does the mixed layer control productivity, but that the relative rate at which turbulent mixing and growth occur can also control bloom initiation. The "critical turbulence hypothesis" posits that slow turbulence can allow for a bloom even when active mixing is below the critical depth. The critical turbulence hypothesis preserves some of the assumptions of the critical depth hypothesis, particularly that growth depends on light exposure and varies with depth and that the loss rate is constant with depth. However, crucially, it does not require a uniform vertical distribution in phytoplankton biomass. When slow turbulence allows for a bloom before restratification, biomass will be highest at the top of the water column.

Previous numerical and analytical studies designed to test the critical turbulence hypothesis have used one-dimensional domains. They have generally used physical set-ups with a constant turbulent diffusivity and model light as a step function, with positive constant growth in one part of the domain and no growth in the other. In terms of biological models, they have modeled growth as exponential with the growth rate a function of depth and include gravitational sinking of phytoplankton cells. Analytical results combined with numerical modeling have found critical length scales of the problem and critical ratios of biological reaction to turbulent time scales for these assumptions [12, 16]. In [36], the authors develop theory and numerical models to link the critical turbulence hypothesis to the shutdown to convective mixing due to the reversal in the sign of air-sea heat flux at the end of the winter. As a consequence of using one-dimensional models, these studies do not explicitly parameterize advection, instead they use a turbulent diffusivity constant and a second-order diffusion term. The only movement of phytoplankton is due to gravitational sinking. In this paper, I use a two dimensional domain for the numerical simulations. This allows me to separately investigate the effects of advection and the effects of diffusion on the model system. I then compare the results on a two dimensional domain to analytic

solutions on a one-dimensional domain.

An alternate hypothesis to light limitation is that ecological mechanisms, in combination with physical forcing, could control bloom timing and the extent of a bloom. The "dilution-recoupling hypothesis" conjectures that deepening of the mixed layer causes an imbalance in predator-prey relations and that a temporary release from predation triggers phytoplankton blooms [3]. Simulation studies related to testing this more ecologically-oriented hypothesis do not include sinking of phytoplankton, but do generally include non-linear growth terms [3, 4, 14]. While hypotheses that relate light exposure to bloom initiation assume that there is no nutrient limitation and no grazing, more ecologically oriented models for bloom initiation assume that nutrient limitation and grazing are both present throughout the year. These growth limitations are can modeled in aggregate using simple non-linear growth [14] or explicitly as individual forcing [5]. In order to unite or even to compare the hypotheses related to the interaction between turbulence and light on the one hand and trophic dynamics on the other, more theoretical modeling of the implications of the critical depth and critical turbulence hypotheses need to be carried out with non-linear reaction terms, which are commonly used in ecology and biological oceanography.

A goal of this work is to increase theoretical understanding of the predictions of the above hypotheses for bloom formation in order to facilitate comparisons to observations. To accomplish this goal, modeling concentration of the light-sensitive chlorophyll as an outcome of the model rather than parameterizing division rate, as the studies on the critical turbulence hypothesis and critical depth hypothesis do, could allow for better comparison to *in situ* observations. In empirical studies, chlorophyll concentrations, rather than division rates, are often observed as a proxy for phytoplankton biomass [27]. Plankton are able to respond physiologically to variation in light exposure by changing their capacity to perform photosynthesis [9]. Chlorophyll can be observed *in situ* and measured using satellite ocean color sensors. Using non-linear models of phytoplankton growth will allow for more direct comparisons between the critical turbulence hypothesis and the dilution-recoupling hypothesis. Finally, few theoretical links between the hypotheses for bloom formation presented above and observed patchiness of plankton blooms have been discussed [25]. Using the numerical results in this paper, I investigate some of the implications of light limitation for heterogeneity of a bloom.

No particular mathematical model is universally applicable for the problem of understanding oceanic phytoplankton bloom formation and evolution. In particular, population dynamics vary across dial and seasonal cycles and different species have fundamentally different population dynamics [17]. Rather than focusing on matching model results to a particular bloom, this paper systematically investigates the mathematical implications of common biological and physical oceanographic assumptions about bloom formation. Bloom characteristics can be described in terms of both physical and biological parameters. The scenarios modeled in this paper are disequilibrium systems with historic dependence. The rate of return to equilibrium is expected to depend on reaction, advection, and diffusion within the system. I aim to disentangle the effects of reaction, advection, and diffusion in each of the models. In order to investigate how non-uniform resource availability and chaotic advection combined

with diffusion can influence plankton growth rates, including high growth conditions that are similar to bloom events, and spatial distribution, I conduct numerical experiments using the fluid model described in the previous section. I systematically introduce different biological models, explaining the motivation behind the modeling assumptions. In addition, I derive and discuss exact solutions for some of the modeling scenarios as a means of discussing the properties of the model that contribute to predictions about plankton bloom dynamics.

2   Aim and research questions

The overall aim of this study is to use mathematical modeling to determine what information spatial heterogeneity of biological tracers can provide about the rates and scaling and phenomenology of biological and turbulent processes and what predictions about spatial heterogeneity of biological tracers can be made given known scaling and phenomenology of biological and turbulent processes.

Mathematical modeling

What results can be obtained using mathematical modeling?
In building a mathematical model to represent ocean processes, I am concerned with both what processes are represented and quantifying the results obtained from the models.
Hypothesis: Biological reactions with different degrees of non-linearity will interact in different ways with advection and diffusion such that meaningfully different conclusions will be drawn about the effects of turbulence on productivity.

Reaction time scales

How does the time scale of biological reactions relative to the time scale of turbulence affect spatial heterogeneity?
Previous theoretical and numerical studies have found that the ratio of characteristic time-scales of the biological and turbulent processes is a key parameter in determining the dynamics of systems controlled by advection, diffusion, and biological reactions [1, 39]. Experiments will vary this ratio to determine the influence this rate has on the distribution of tracer concentrations given different models of biological processes and idealized flow fields. Analytic results can also be derived for the theoretical influence of reaction rate on tracer probability distribution functions.
Hypothesis: Spatial heterogeneity will be increased with faster biological reactions relative to mixing.
Hypothesis: Diffusion affects the time to equilibrium and patchiness in systems with non-linear reactions.

Ecosystem models

How are predictions about the interaction between light exposure and turbulence affected by the inclusion of higher trophic levels?

The dilution-recoupling hypothesis diverges entirely from the predictions of the **Hypothesis:** In mathematical models, higher trophic levels will interact with spatially and temporally heterogenous phytoplankton populations such that there is a dependence between the effects of turbulence on primary productivity due to light exposure and higher-level ecosystem dynamics.

3   Lattice model of advection-diffusion

The large scale distribution of plankton is modeled by an advection-reaction-diffusion type equation. I extend the use of a computationally efficient and easy to implement fluid dynamics model designed to study advection-diffusion systems that incorporates important theoretical aspects of fluid flow. This model can be easily modified in order to control the strength of both advection and diffusion (including scenarios with no diffusion) as well as the time scale and the length scale of the reactions and resource availability. These attributes are important in order to separately investigate the impacts of advection, diffusion, and reaction on the system. In this section, I outline the implementation of a model of advection and diffusion and investigate the impact of the advection model on the properties of a non-reactive tracer.

The density field of nutrient or plankton mass per fluid volume, denoted as N($\mathbf{r}$,t), is continuous and two dimensional over the ocean surface or in a vertical profile. The velocity field, v($\mathbf{r}$,t), is two-dimensional, incompressible, and varies in time. Mixing is modeled as diffusion with inverse Peclet number Pe^{-1}. The Peclet number is a non-dimensional measure of the relative strength of advection to diffusion. $Pe = \frac{uL}{\kappa}$ where u is the fluid velocity, L is the length scale, and κ is diffusivity. Reactions can be included using a number of different functions, denoted by the function F and described in the following sections. The non-dimensional Damkohler number, Da, is a ratio of the advective and reactive time scales. The function F determines the rate of change of plankton mass per fluid volume due to reactions. The Peclet number and Damkohler number are discussed further in section 3.1. The overall advection-reaction-diffusion system is:

$$\frac{\partial \mathbf{N}}{\partial t} + \mathbf{v} \cdot \nabla \mathbf{N} = DaF(\mathbf{N}; \mathbf{r}) + Pe^{-1}\nabla^2 \mathbf{N} \tag{1}$$

where the vector $\mathbf{N} = \{N, P, Z\}$ represents, nutrients, phytoplankton, and zooplankton, the components of a ecosystem models

3.1   Dimensional analysis and non-dimensional parameters

The general equation for an advection-reaction-diffusion system in dimensional parameters, with [N] representing the mass of plankton or nutrients per unit volume is

$$\underbrace{\frac{\partial N}{\partial t}}_{\text{[N] time}^{-1}} + \underbrace{\nabla \cdot (uN)}_{\text{[N] length}^{-1}\times\text{length time}^{-1}} = \underbrace{\kappa\nabla^2 N}_{\text{length}^2\text{time}^{-1}\times\text{[N] length}^{-2}} + \underbrace{f(N)}_{\text{[N] time}^{-1}} \tag{2}$$

In order to fully explore the parameter space of fluid dynamics and biological properties and to generalize the results, I use non-dimensional parameters from here forward. There are two commonly used non-dimensional parameters for advection-reaction-diffusion systems, the Peclet number (Pe) and the Damkohler number (Da), both of which appeared earlier in equation 1. The Peclet number is the ratio between the strength of advection and the strength of diffusion. It is defined as $Pe = \frac{uL}{\kappa}$ where L is the length scale of the problem. In this case, L is defined to be the mixed layer depth. In later sections, when the advection-reaction-diffusion system is used to model biological tracers, the Peclet number incorporates exchange of biological tracer between adjacent water parcels due to random motion, including molecular diffusion, unresolved turbulence, and random swimming by motile plankton.

The Damkohler number is a ratio between reactive and advective time scales. It is defined as $Da = \frac{u}{L}\gamma$ where γ is the reaction rate. In a simple exponential growth model, γ is the specific growth rate. Even when the reactions are not exponential, the Damkohler number can be diagnosed by considering the ratio of the reaction term to the effects of the advection term, either during an exponential growth phase, or averaged over the time until equilibrium of the reaction. It is evident that Pe and Da are related through the advective time scale. In order to convert between the non-dimensional scales used in the following simulations and physical scales, specify either the time step of the model (T),which determines the advective timescale, or the reactive time scale (γ) and either the length scale of the model (L) or the velocity scale of the model (u) and the other two parameters will be determined.

In the model simulations, I have a third non-dimensional parameter, t^*. t^* is the ratio between the model time step, defined as $T = \frac{L}{u}$, and the time after which the velocity field is randomized (T_{random}). This quantity parameterizes temporal velocity variance. Physical reasons for differing velocity variance in the open ocean include wind variability and internal waves. In this work, I use a consistent $t^* = 3$.

3.2 Advection-diffusion model

A turbulent mixed layer is modeled using numerical simulations of a system that qualitatively reflects ocean turbulence on a two dimensional discrete grid. In this project, I modify a lattice advection algorithm developed by [32].

3.2.1 Chaotic advection

The fluid flow model is discretized in both space and time. As in the algorithm in [32], advection is simulated by mapping parcels tagged with tracer concentration bijectively using an area preserving map at each time step.

$$
\begin{aligned}
x &\mapsto x + u_n(y)\Delta t \\
y &\mapsto y + v_n(x)\Delta t
\end{aligned}
\tag{3}
$$

With velocities determined by the streamfunction

$$
\Psi = U_1 \cos(x + \psi_n) \cdot f(z) + U_2 \cos(z + \phi_n)
\tag{4}
$$

9

Where ϕ_n and ψ_n are independent random phase shifts chosen on the interval $[0\ 2\pi]$ so that all particles will be able to come in contact with each other. Generating velocities from a streamfunction ensures incompressibility. In the model developed by [32], the flow in the x direction is not correlated with the flow in the y direction and the model has doubly periodic boundary conditions. This is equivalent to setting the function $f(z)$ to a constant in equation 4. With $f(z) = 1$, the x and z model velocities are

Step 1:

$$
\begin{aligned}
u_n(y) &= U_1 \sin(y + \phi_n) \\
v_n(x) &= 0
\end{aligned}
\tag{5}
$$

Step 2:

$$
\begin{aligned}
u_n(y) &= 0 \\
v_n(x) &= U_2 \sin(x + \psi_n)
\end{aligned}
\tag{6}
$$

This model produces chaotic trajectories and is consistent with the scaling laws obtained from theoretical studies on fluid flow. Snapshots of the spatial distribution of tracer with no reactions are shown in figure 1. Figure 1 shows the result of chaotic advection-diffusion. Without diffusion, the blue and yellow blocks from the left panel of figure 1 would appear to be randomly distributed after advection for 100 time steps.

I modified the lattice model presented by [32] to a similar exact Lagrangian
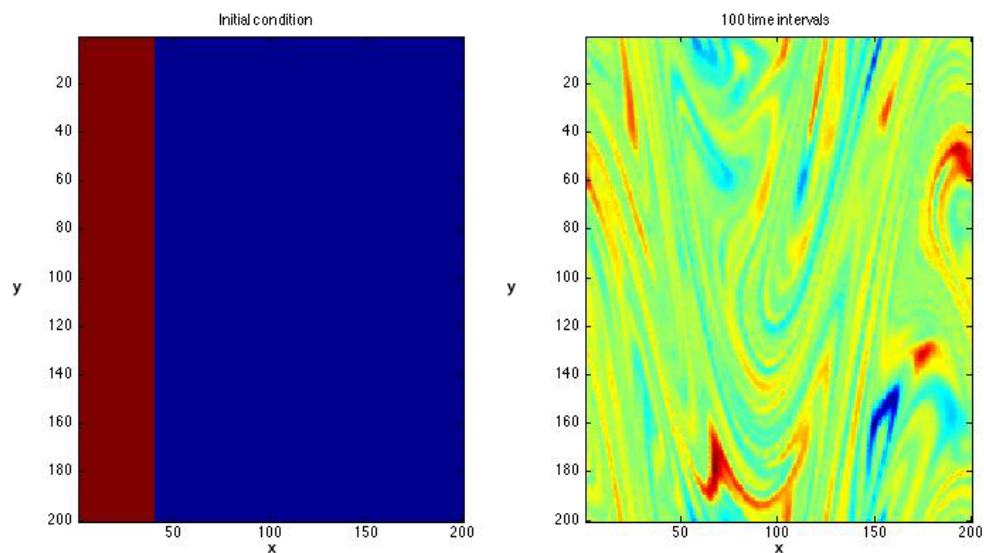

Figure 1: Initially, a small amount of tracer is added to the left hand side of the domain (left). After 100 time steps, the turbulent mixing has reduced the variance (right)

model with closed boundaries by defining

$$
f(z) = z(1-z)^2
\tag{7}
$$

For a domain size of 1 in the z-direction. The shape function (equation 7) was chosen based on the conditions that there is no normal flow through the boundaries (i.e. $f(z = 0) = 0$ and $f(z = 1) = 0$, resulting in the streamfunction equal to zero at the boundaries) and no tangential flow at the bottom boundary (i.e. $f'(z = 1) = 0$). The condition that the first derivative goes to zero at the layer base avoids large jumps in diffusivity at $z = 1$ as discussed in [18] for implementation in the Community Ocean Vertical Mixing parameterization (CVMix).

The the velocities in each direction that result from this model are

$$\frac{dx}{dt} = u_n(x, z) = \Psi_y = 2\cos(x + \psi_n) \cdot f'(z) + \sin(z + \phi_n) \tag{8}$$

$$\frac{dz}{dt} = w_n(x, z) = \Psi_x = 2\sin(x + \psi_n) \cdot f(z) \tag{9}$$

The velocity fields are mapped in space in figure 2a. Since u_n and w_n, as defined in equations 8 and 9, respectively, are continuous, the parcels must be coerced onto to the regular lattice grid at each time step. The problem of optimally fitting a set of parcels onto a grid is a linear assignment problem. A linear assignment algorithm finds a bijection that maps set A to set B while also minimizing the total value of a cost function. In this lattice model problem, the cost function for each parcel i is defined as the distance between the regular grid points (x_g, z_g) and the parcel coordinates after being transformed by the continuous velocity field by the map defined in equation 3.

$$C_i = \sqrt{(x_i - x_g)^2 + (z_i - z_g)^2} \tag{10}$$

In the case with $f(z)$ constant, the cost function was minimized by simply rounding the parcel position in each direction to an integer value. For the fluid model with closed boundaries, I map parcel locations to the grid using the Jonker-Volgenant algorithm [21]. A schematic showing the motion of parcels during one time step is shown in figure 2b. On average, parceled are mapped to very close by grid points (cost function average values are less than 0.5). The highest values of the cost function are in the areas with the greatest velocity (compare figure 2c to figure 2a).

3.2.2   Diffusion

The advection scheme alone models the case where $Pe \to \infty$. Diffusion is added using a five-point smoother, so that a range of Peclet numbers are possible for each grid size.

$$\mathbf{N}_{i,j}(t + 1) = \frac{1 - b}{4}(\mathbf{N}_{i+1,j}(t) + \mathbf{N}_{i-1,j}(t) + \mathbf{N}_{i,j+1}(t) + \mathbf{N}_{i,j-1}(t)) + b\mathbf{N}_{ij}(t) \tag{11}$$

where b is a parameter that controls the strength of diffusion. If $b = 0$, equation 11 is a four point smoother and diffusion is grid-size dependent. If $b = 1$, then there is no diffusion (i.e. $Pe \to \infty$). Diffusion is applied after one Δt time step. Because the velocity profile varies with depth (figure 2a), the Peclet number also varies with depth, with peaks at intermediate depth due to large velocities and peaks at shallow and deep parts of the model due to low gradients, and consequent low rate of change in tracer concentration due to diffusion.
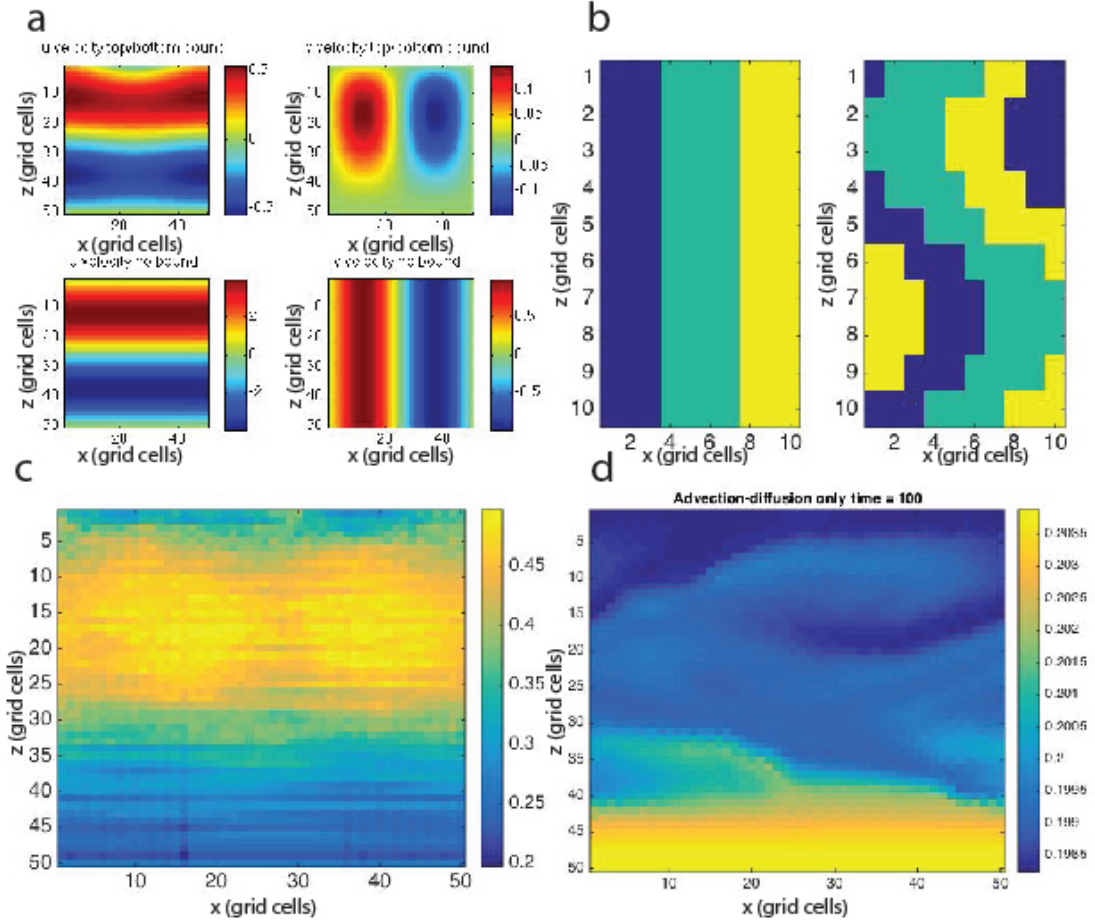
Figure 2: Illustrations of the properties of the lattice model of advection and diffusion with closed boundaries. **a.** Example velocity fields with no phase shift ($\phi_n = \psi_n = 0$), as given by equations 8 and 9 (top) and equation 18 and 20 (bottom). In the model, the phase shift (ϕ and ψ) are random variables chosen every 6 time steps. **b.** Schematic showing rearrangement of fluid parcels by continuous velocity fields (equations 8 and 9) and linear assignment. **c.** Mean cost function (C_i) over 100 replicate simulations. **d.** Spatial distribution of tracer after 100 time steps of mixing and stirring starting from an initial tracer gradient with high concentration at the bottom and low concentration at the top
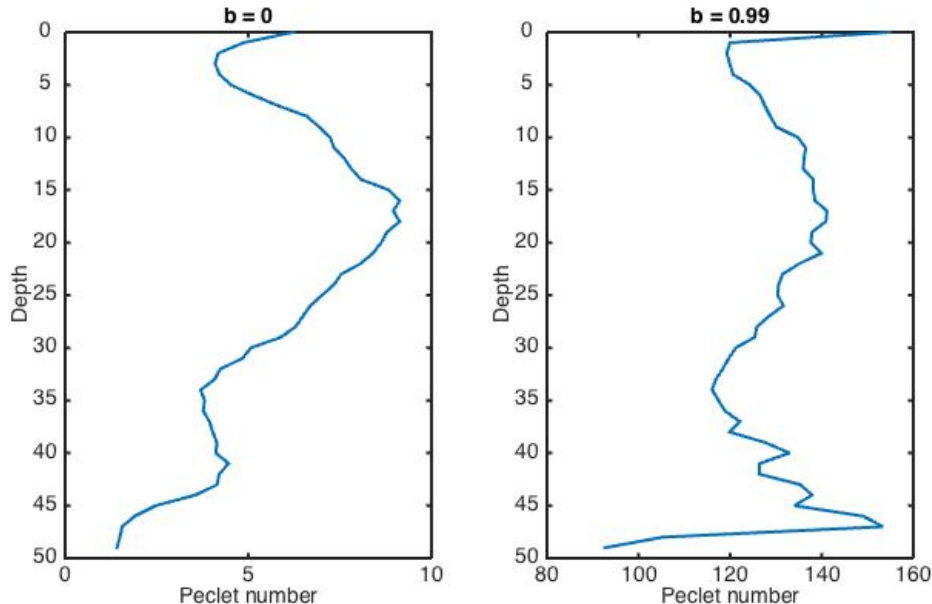
Figure 3: Peclet number distribution with depth for strong diffusion (b = 0) and weaker diffusion (b = 0.99) on a 50 by 50 grid. b controls the amount of concentration each parcel exchanges with neighboring parcels in the 5-point smoother defined in equation 11

3.2.3   Production of tracer variance

With no reactions, the mean tracer concentration over the entire spatial field predictably stays constant. The variance decays to zero (machine precision) because of the inclusion of diffusion (figure 4). The variance decays exponentially, as described in [33]. The similarity between figure 4 and figure 4 is one test that the fluid flow model used in this paper reproduces the model developed by [33]; more details about the model can be found in that paper. The rate of decay is related to the typical Lyapunov exponent of the mixing and the average concentration gradient between neighboring particles rather than the strength of diffusion. This understanding of background tracer variance will be utilized when interpreting results that include forcing from biological reactions.

The flow field is non-divergent so the rate of change of tracer variance without forcing from a reaction is

$$\frac{\partial}{\partial t}\frac{1}{2}N^2 + u \cdot \nabla \frac{1}{2}N^2 = NPe^{-1}\nabla^2 N \tag{12}$$

In the case with periodic boundaries, the variances for the basins with different initial conditions converge. The results in figure 4 are consistent with those found by Pierrehumbert when using the same model [32]. The results from Pierrehumbert (2000) are shown in figure 5. The no flux boundary conditions introduce spatial strusture in tracer variance. Snapshots of the spatial distribution of tracer with no reactions and
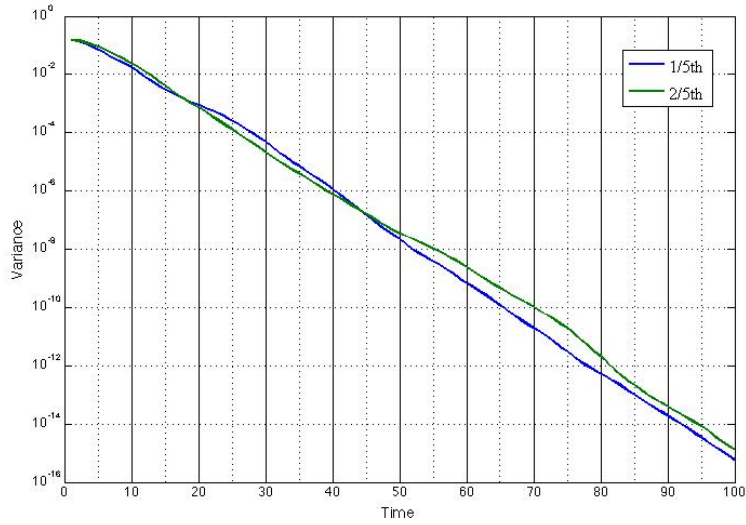
Figure 4: Tracer concentration variance with tracer coming from one side, covering either 1/5th or 2/5ths of the area. Concentration variance of a tracer representing nutrients (N) is basin integrated and calculated as $\int\int(N^2- <N>^2)dxdy$ where angle brackets denote the spatial average.
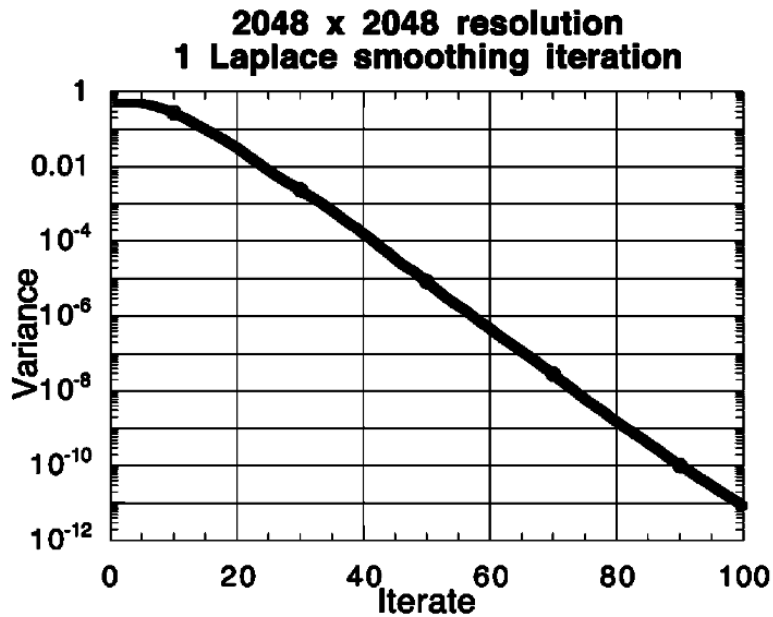

Figure 5: Pierrehumbert (2000) figure 3. Tracer concentration variance as a function of time.

an initial gradient in tracer from bottom to top are shown in figure 2d. The mean tracer concentration variance as a function of depth can be fit with a cubic function that peaks in the middle of the grid, where velocities are also the highest (figure 6). As can be seen in figure 2d, this is the region where filaments are most likely to form due to advection.

Consequently, the initial decay of tracer variance depends on the initial conditions (figure 7). Larger gradients are generated by advection when the tracer is initially randomly distributed or initially on the sides, which are periodic boundaries. After the initial period, variance decays exponentially at the same rate for all initial conditions. The tracer concentration variance ultimately decays to zero. After an
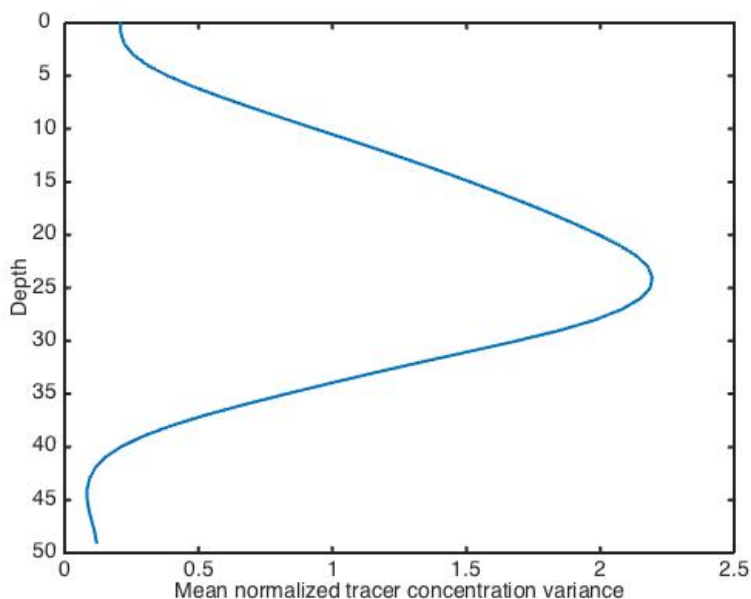

Figure 6: Variance with depth on a 50 by 50 grid. The mean normalized variance is the mean for each depth over 3000 iterations, normalized by the whole grid mean variance for each iteration. This figure produced with random initial tracer concentration.

initial adjustment period to smooth out gradients related to the initial conditions, the rate of decay of concentration variance is related to the Peclet number, the Lyapunov exponent of mixing (λ_m), and the domain size. Gradients are amplified exponentially as $\delta = e^{-\lambda_m t^*}$ for non-dimensional λ_m. While strain amplifies gradients, diffusion smoothes them out. The scale at which strain and diffusion are balanced is

$$l_* = (\lambda_m Pe)^{-\frac{1}{2}} \tag{13}$$

As a result of this relationship, for low Peclet number, the characteristic length scale of mixing is the domain size. The characteristic length scale of mixing is smaller for larger Pe, as a result, the variance slope is smaller for larger Pe (figure 8).
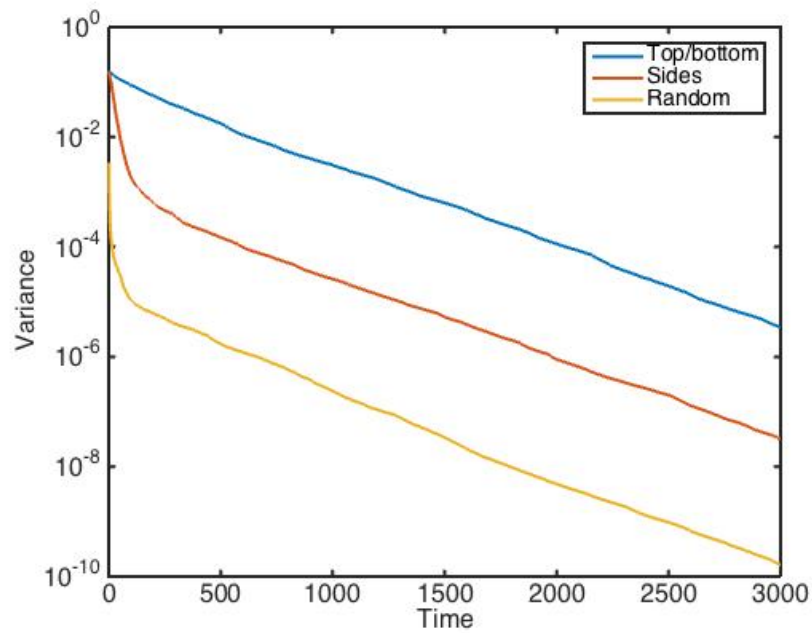
15

Figure 7: Mean variance as a function of time on a 50 by 50 grid. Each line represents a different initial condition.
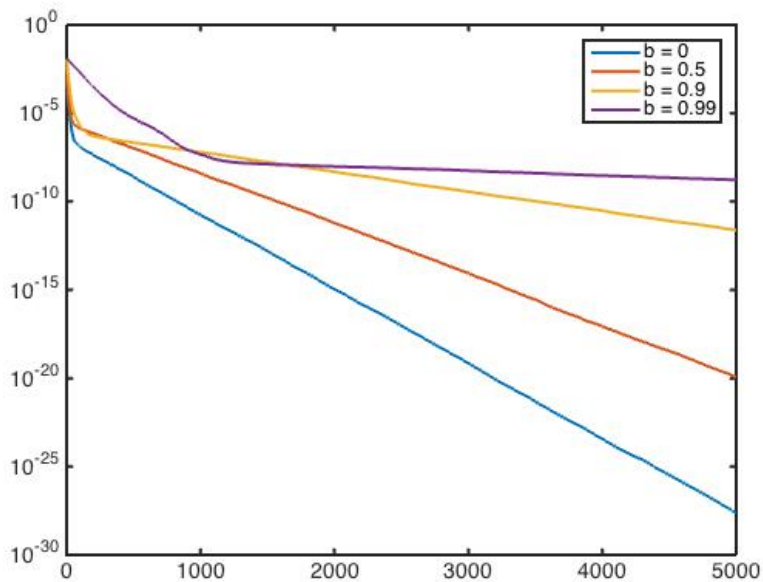

Figure 8: Variance with depth on a 50 by 50 grid. The mean normalized variance is the mean for each depth over 3000 iterations, normalized by the whole grid mean variance for each iteration. This figure produced with random initial tracer concentration.

3.2.4   Comparison to *in situ* measurements

I verify the model velocity field using measurements from Lagrangian floats. The float is carried in the mixed layer along with a water parcel. When investigating the influence of turbulence on the growth of plankton due to exposure to different light conditions, we are most interested in the vertical profile of plankton. The details of the float design are described in [22]. I try to match the statistics of this float from one particular time period (August 25th, 2012 to October 3rd, 2012) and place (North Pacific) to the statistics of the model with closed top and bottom boundaries. Namely, when matching the mixed layer depth (spatial scale) and average velocity, I verify that the velocity profile in the model has the same velocity variance and autocorrelation as fluid parcels in my model have similar depth profiles.

Velocity variance

The velocity variance from flow field defined in equations 8 and 9 nearly matches the expectation from empirical distributions (figure 9). The shallower peak velocity in the empirical data (figure 9a) is expected due to wave-driven Langmuir mixing, which is not incorporated in the idealized fluid model.

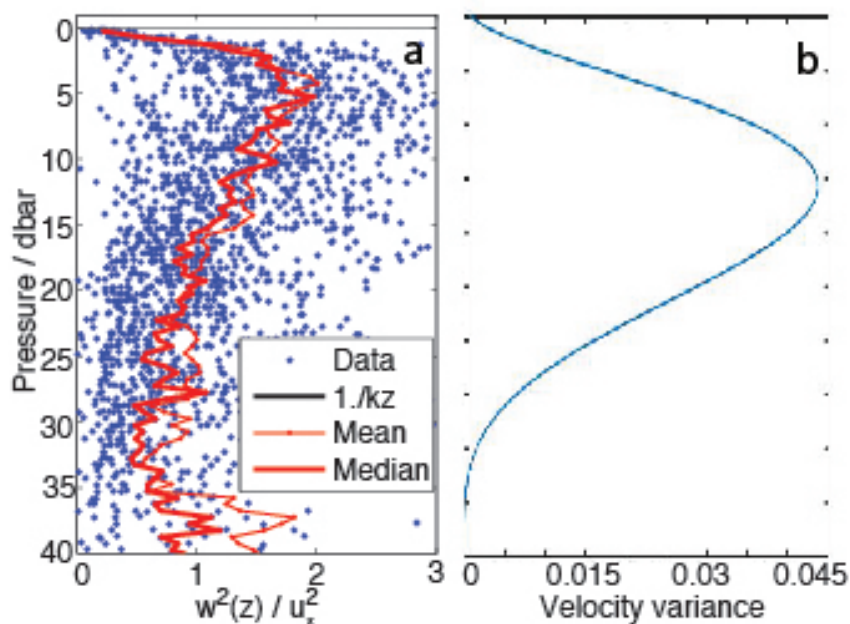**Calculations to compare model and observed depth profiles**

Figure 9: (a). Velocity variance with pressure as calculated from Lagrangian float measurements (personal communication, D'Asaro 2015). (b). Velocity variance with depth on a 50 by 50 grid. The variance is the mean for each depth over 3000 iterations. This figure produced with random initial tracer concentration.

The median mixed layer depth (H) in the float data is 22 meters. The vertical velocity variance is known to scale with wind stress forcing [10]. I use the following relationship (equation 14) to standardize for the effects of wind forcing on vertical

velocity (w).

$$\frac{w^2_{observed}}{w^2_{standard}} = \frac{u^{*2}_{observed}}{u^{*2}_{standard}} \tag{14}$$

where for wind stress τ_{wind} and water density ρ, $u^* = \frac{\sqrt{\tau_{wind}}}{\rho}$. Using the typical values of $\tau_{wind} = 0.1$ N/m^2 and $\rho = 1000$ kg/m^3, I obtain a standard wind forcing $u^*_{standard} = 0.01$ m/s. This value is very close to the median u^* observed from Waverider, 0.0099 m/s, so the rescaling in 14 is not needed. I scale the vertical velocities in my model to have the same time and space mean variance as the observed vertical velocities ($w^2_{observed} = 1.67 \times 10^{-4}$ m^2/s^2) (figure 9).

The model time scale, which depends on the length scale and velocity scale is $\frac{H}{w} = \frac{22}{0.0129} = 1,705$ seconds or 28.4 minutes, so I compare vertical positions between the model and the float observations at 28.4 minute intervals. The vertical velocity autocorrelation timescale, calculated as the first zero crossing time of the autocorrelation curve, is 600 seconds. I randomize the velocity field every 3 model time steps in order to have the same autocorrelation time scale. The floats record vertical position every 30 seconds on average (figure 10).

In general, the model has smaller changes in depth in a given time interval (smaller $\frac{dz}{dt}$) than the float. This is likely complicated by the large grid cells in the model (0.44 meters/grid cell with a 22 meter mixed layer) (figure 10).

Ranges for non-dimensional parameters

Reasonable constraints on Da can be made by comparison to field studies. For example, [11] used physical oceanographic measurements to estimate that the time scale for vertical displacement in the open ocean is 0.5-100s h$^-1$. Specific growth rates of plankton populations have been recorded in field and *in situ* measurements in bloom and non-bloom conditions [7,13] to range from 0.0033 h$^-1$ to 13 h$^-1$. The ratio of these timescales gives Damkohler numbers in the range of 3.3·10^{-5} to 7.5. Theoretical calculation of molecular diffusivity provides an upper bound on the Peclet number. With average mixed layer velocity of 0.1 m/s and mixed layer depth of 50 meters and molecular diffusivity of 10^{-7} m^2/s, a typical Peclet number in the ocean mixed layer would be 5×10^6. Smaller values of Pe incorporate unresolved turbulence and random swimming by plankton.

3.3 Discussion

The simple model of advection and diffusion presented in [32] is efficient to implement and meets many of the requirements for a model of fluid flow. In particular, it is an exact Lagrangian model that allows control over the strength of diffusivity. In this section, I confirmed that my implementation matches that of [32]. However, because there is no correlation between movement in the horizontal direction with that in the vertical direction, that model can only be used for a system with doubly periodic boundary conditions. I have adapted the model in [32] for use in exploring biological productivity in a vertical section of the mixed layer by adding closed top and bottom boundaries and compared the model depth profiles with the depth profile of a float in the North Pacific. I then synthesized some of the relevant properties of
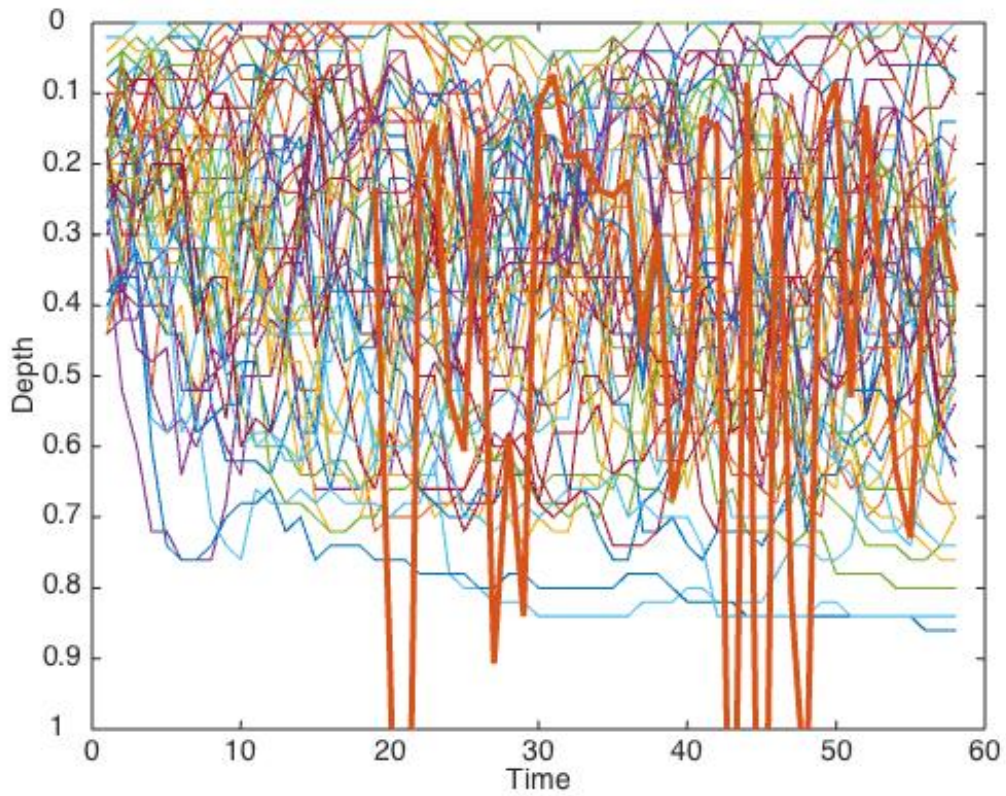
Figure 10: Comparison of float depth with water parcel depths in the model. Depth is measured as percent of mixed layer; 0 is the surface and 1 is the base of the mixed layer. Run with a 50 by 50 grid. The float is the bold line.

the model for analysis of future experiments including exponential decay of variance of a passive tracer and dependence of the rate of decay on the Lyapunov exponent of mixing and average concentration gradient between neighboring particles.

The impact of advection model on a biological tracer could be explored further by using a more realistic flow field or by altering the advection to have multiple modes leading to stratified turbulence. In addition, although this two dimensional model allows for full investigation of the predictions of the hypotheses for bloom formation outlined above, the critical depth, critical turbulence, and dilution-recoupling hypotheses, turbulence in three dimensions could also have important implications for bloom formation and a similar approach to understanding the fundamentals of advection, diffusion, and biological reactions in a three-dimensional system could also yield important insights [25].

4 Reacting tracer fundamentals

Using simple spatially uniform reactions, in this section I discuss the interaction between reactions and the advection-diffusion model, focusing on tracer variance and measures of spatial heterogeneity. In this section, I further define some of the baseline properties of a reaction-advection-diffusion system before adding spatial heterogeneity.

4.1 Exponential decay

In order to test the impact of underlying exponential decay of the tracer variance in a case with a biological reaction, I used a simple model in which a tracer (representing nutrients) decays exponentially. This simple model of nutrient uptake occurs without explicitly incorporating biological growth. For this model, the reaction function is

$$F(N; \mathbf{r}) = -\gamma N \qquad (15)$$

In this case, the mean tracer concentration decays exponentially with constant Da. Variance decays exponentially as well (figure 11). The mean of the non-reacting case multiplied by $e^{-\gamma t}$ is the same as that of the exponential decay case. When the variance of the non-reacting case is multiplied by $e^{-2\gamma t}$, it is the same as that of the exponential decay case (figure 11). This result demonstrates that the background effects of fluid flow on reactive tracers can be disentangled in certain cases. It is expected that transport will have no effect on a biological reaction when there is no spatial heterogeneity due to other terms in equation 1. For example, a population could have spatially heterogenous growth due to spatially heterogenous nutrient availability or spatially heterogenous loss due to diffusion of predators or competitors. In what follows, I develop this idea further by solving for tracer concentrations in the moving frame of a reaction-advection system.
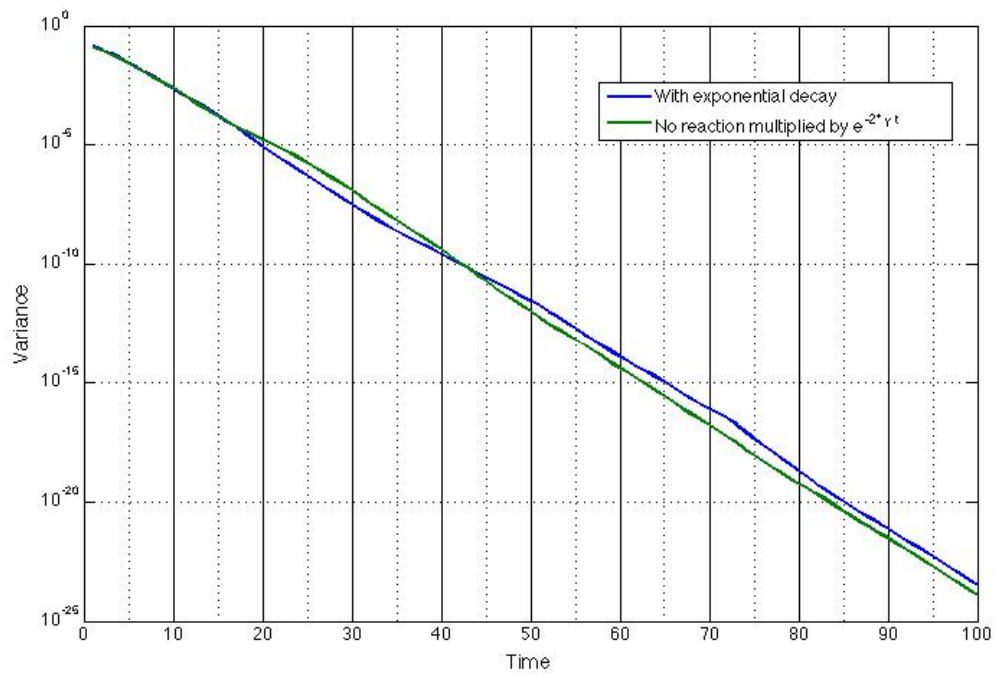
Figure 11: Evolution of spatial variance of an exponentially decaying tracer with time. The rate of exponential decay is $\gamma = 0.1$. Initially, the tracer covers $1/5^{th}$ of the basin.

4.2 Method of characteristics solutions for spatially uniform reactions

When there is no spatial dependence in the reaction term and no diffusion term, a tracer follows trajectories and changes concentration due only to the reaction term, independently of the advection terms. Similarly, advection of the tracer is independent of the tracer concentration (passive transport).

This is demonstrated by returning again to the simplest tracer transport equation, where the material derivative is zero. I find expressions for the trajectories of tracer in the fluid. I begin by solving the equation for transport of a non-diffusive and non-reactive tracer $N(x, t)$ in one dimension.

$$\frac{DN}{Dt} = \frac{\partial N}{\partial t} + U\frac{\partial N}{\partial x} = 0 \tag{16}$$

Equation 16 is similar to a conservation of mass statement for a tracer in one dimension. This equation can be solved using the method of characteristics. Using the chain rule:

$$\frac{dN}{dt} = \frac{\partial N}{\partial t} + \frac{\partial N}{\partial x}\frac{dx}{dt} \tag{17}$$

By comparison with equation 16

$$\frac{dN}{dt} = \frac{\partial N}{\partial t} + \frac{\partial N}{\partial x}U = 0$$

and the system reduces to the coupled set of ODEs,

$$\begin{aligned} \frac{dN(x,t)}{dt} &= 0 \\ \frac{dx}{dt} &= U(x,t) \end{aligned} \tag{18}$$

Solving these equations depends on the form of $U(x, t)$. For example, if $U(x, t) = U_0$ is constant, $x = x_0 + U_0 t$ and the evolution of the concentration has the general form $N(x, t) = f(x - U_0 t)$.

Adding a reaction term to equation 16 results in a reaction-advection system where tracer concentration can change along trajectories. In this solution, I use the general reaction term $F(N)$. In the last section, I used an exponential decay, i.e. $F(N) = -\gamma N$.

$$\frac{DN}{Dt} = \frac{\partial N}{\partial t} + U\frac{\partial N}{\partial x} = F(N) \tag{19}$$

When the reaction term does not depend explicitly on space or time, a reaction-advection problem can be solved using the method of characteristics. Comparing equation 17 to equation 19, I get the coupled set of ODEs,

$$\begin{aligned} \frac{dN(x,t)}{dt} &= F(N) \\ \frac{dx}{dt} &= U(x,t) \end{aligned} \tag{20}$$

This generalizes to non-divergent two dimensional flow as well

$$\frac{DN}{Dt} = \frac{\partial N}{\partial t} + U_x\frac{\partial N}{\partial x} + U_y\frac{\partial N}{\partial y} = F(N) \tag{21}$$

$$\frac{dN}{dt} = \frac{\partial N}{\partial t} + \frac{\partial N}{\partial x}\frac{dx}{dt} + \frac{\partial N}{\partial y}\frac{dy}{dt} \qquad (22)$$

Comparing equation 21 and 22, I get a system of ODEs

$$\begin{aligned} \frac{dN(x,y,t)}{dt} &= F(N) \\ \frac{dx}{dt} &= U_x(x, y, t) \\ \frac{dy}{dt} &= U_y(x, y, t) \end{aligned} \qquad (23)$$

Thus, without diffusion, the transport of a reactive tracer that has no spatial dependence in the reaction term can be easily disentangled from the reaction of that tracer. While the processes occur together, they do not interact. In this case, the ratio of time scales of reaction and advection (Da) has no implications for the progress of the reaction in a Lagrangian frame. With large Pe and a single reacting population, the results are expected to be similar to first order when diffusion is included.

4.3 Saturating reactions

The next simplest model of exponential decay involves the decay of a tracer until it reaches a pre-determined background concentration, which I call the saturating model.

$$F(N; \mathbf{r}) = \gamma(N^* - N) \qquad (24)$$

While diffusion is not expected to change the equilibrium concentration, it may have transitory effects while the population progresses to equilibrium, when there are still concentration gradients present. Numerical results demonstrate that in a system with a saturating reaction of the form presented in equation 24, mixing does not impact the time to reach equilibrium (table 1). In this numerical experiment, the lattice had a homogenous, non-advecting and non-decaying carrying capacity of either N^* = 0.1 or N^* = 0.3. I also ran simulations with an inhomogenous, non-advecting and non-decaying carrying capacity with mean of N^* = 0.11. The tracer (phytoplankton) was placed on the lattice in various configurations, but all with a mean starting value of 0.2. Equilibrium is determined when the difference between the tracer value and the mean carrying capacity ($< N^* >$) was less than 10^{-6}.

Table 1: Saturating model time to equilibrium

γ	With turbulence	Without turbulence
0.01	461	461
0.1	47	47
1	4	4
10	1	1

Many methods for measuring spatial heterogeneity are available including probability density functions (PDFs) and spectral analysis. When using these methods,
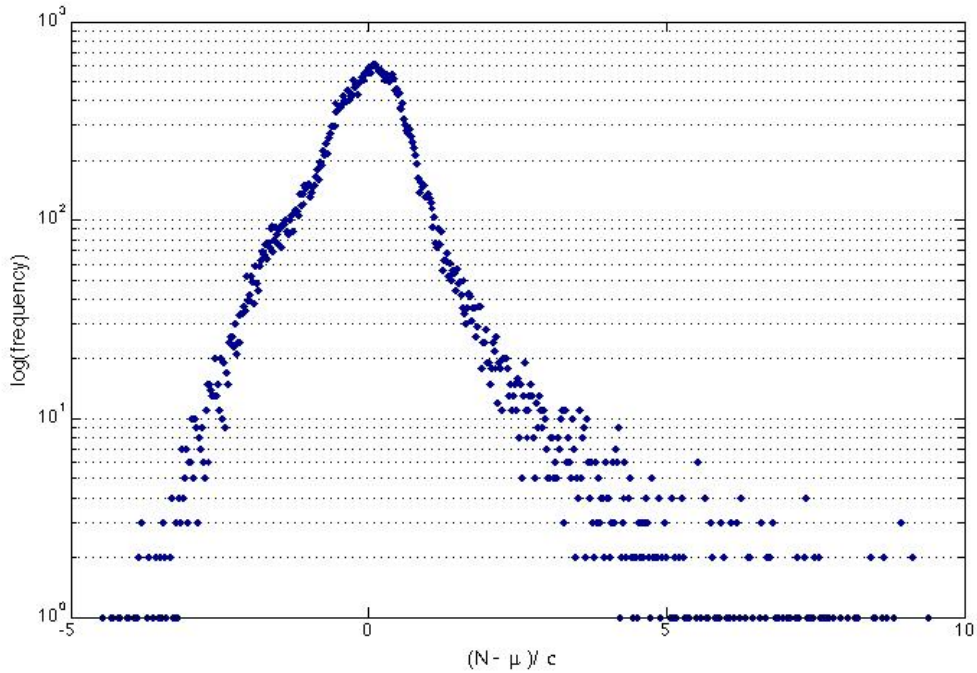
Figure 12: Histogram of normalized tracer concentration after 100 time steps with no reactions

one presents the variance as a function of the length scale and interprets great spatial heterogeneity if more of the variance is at the smaller length scale. [24]. I only looked at the PDFs of tracer concentrations for my simulations. In the case of no reactions where the tracer concentration decays by advection and diffusion, the PDF is not Gaussian [32]. The tails of the distribution are larger and more skewed than those of a Gaussian PDF (figure 12).

Once at equilibrium, the PDFs of the saturating reaction are not Gaussian and are skewed to the right. With no reactions and with a saturating reaction, the higher order moments of the distribution are large and vary widely as the reaction progresses.

Using saturating reactions, I have demonstrated diffusion does not affect the timescale of a spatially homogenous reaction, I have further established that the first two moments of a distribution, the mean and the variance, are reasonably good descriptors of the properties of these biological population in turbulent flow.

4.4   Discussion

The results of this section suggest that mixing alone cannot be responsible for altering the measured properties (mean and variance) of biological dynamics in ocean systems. There must be some other mechanisms operating at a scale different from that of mixing that cause heterogeneity in a parameter that is important for biological growth. I consider these other mechanisms in the chapters that follow.

With simple reactions of the form $F(u)$ (no spatial dependence), the reactions
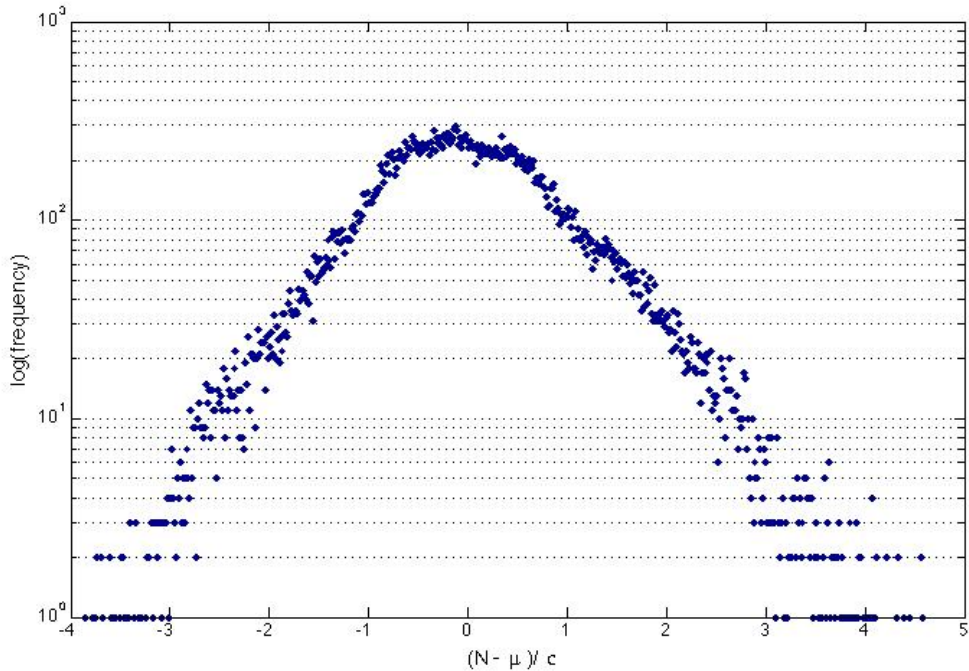
Figure 13: Histogram of normalized tracer concentration forced by a saturating reaction with $\gamma = 0.1$ after 100 time steps

can be disentangled from advection. This result was derived analytically using a method of characteristics solution. In practice, in the simulations in which the reactions had no spatial dependence, the effects of the reaction can be disentangled from the effects of advection and diffusion. It was shown numerically that diffusion does not affect the decay of tracer variance differentially when a reaction accelerates decay to zero, nor does it differentially affect the time to equilibrium in a reaction that progresses to a non-zero steady state.

Although the PDFs are not Gaussian for either a non-reactive tracer or a tracer with a saturating reaction source term, they can be relatively well described with the Gaussian parameters of mean and variance, except for extreme events, which may be interesting to investigate. These Gaussian parameters provide useful information about the system. In the simulations that follow, I use mean and variance to investigate the basic impacts of stirring on well understood models of biological processes. I selected these parameters to describe bloom dynamics because they most simply fit the predictions of theoretical models of phytoplankton bloom evolution. A detailed analysis of higher moments is beyond the scope of this work.

5 Light-dependent non-linear growth

In the previous section, I demonstrated that spatial heterogeneity is necessary to generate patchy plankton distribution. In modeling the onset of a phytoplankton

bloom, it might be reasonable to assume that the limit, or carrying capacity, on chlorophyll concentration is proportional to light availability, but affected by losses due to nutrient limitation and grazing. I model loss as a self-limiting process without explicitly modeling a mechanism for growth limitation at high plankton concentrations. Even while using this simplifying assumption, the form of phytoplankton growth can be selected based on a number of other assumptions about population growth.

In order to investigate the effects of assumptions about the form of a biological reaction on conclusions drawn about population dynamics, I compare and contrast the results from using two non-linear models of plankton growth of differing degree. Although the nonlinear models I use in this section are commonly used and simple to interpret biologically, they are not mathematically simple. I resort to using one-dimensional models to find analytical solutions.

Mixing can have two main effects on a system, affecting the length scale or the time scale of population dynamics. These two effects fundamentally underlay the critical depth hypothesis and critical turbulence hypothesis, respectively. Mixing can alter the temporal dynamics if the time scale of mixing is such that it interrupts progress to equilibrium in local populations. The concept of time scales of reactions interacting with time scales of transport processes has been studied in chemical reactions by modifying the timescale of reactions relative to the timescales of advection and diffusion [28]. The relative importance of local growth and mixing can also affect the spatial distribution of a population. Phytoplankton cells will grow faster where resources are abundant, but transport processes will mix cells between areas of high and low concentration. At the limit of very fast mixing, cells will be uniformly distributed regardless of resource availability, according to the assumptions of the critical depth hypothesis. In this section, I use the fluid model with closed top and bottom boundaries in order to simulate zero flux in a vertical column. Light is modeled as an exponential decay, with highest light levels at the top of the section.

5.1   Temporal heterogeneity of equilibrium dynamics

Introducing spatial variation in one of the two interacting variables (nutrients and phytoplankton) allows me to create models with non-trivial effects of stirring. I create an inhomogeneous carrying capacity field for the plankton that does not vary with stirring. Light availability, which is an explicit function of z, is modeled as exponential decay with e-folding depth $\frac{1}{\lambda}$ [8].

$$N(z) = e^{-\lambda z} \tag{25}$$

From a Lagrangian perspective, mixing brings a fluid parcel and the phytoplankton it contains into contact with different carrying capacities at different times. In this way, the spatial heterogeneity becomes temporal heterogeneity, depending on the perspective. I use a logistic growth model for plankton in this section and solve it numerically using a Runge-Kutta method, ode45 in Matlab.

$$F(P; \mathbf{r}) = \gamma P\left(1 - \frac{P}{K(\mathbf{r})}\right) \tag{26}$$

In the above model, K($\mathbf{r}$) is the carrying capacity and does not change throughout time. I carried out a simulation with plankton starting at a uniform concentration and $K(\mathbf{r}) = N(z)$ (figure 14). Physically, this setup could represent different carrying capacities because of different light availability at different depths. λ varies seasonally and with the dial cycle. I use a simple formulation of the Damkohler number

$$Da = \left\langle \frac{\bar{u}}{L} \right\rangle \gamma \tag{27}$$

Where γ is the exponential growth rate in equation 26, the over bar represents the time mean and the angle brackets represent the spatial mean. The advantage of this formulation is that Da is a simple summary statistic that does not vary with time and space. However, as discussed below, alternative formulations may be more appropriate for representing the timescales of non-linear reactions in chaotic flows.

In this case, the PDF of plankton concentration is multimodal. At low growth, the PDF has three peaks. As γ increases, there are many low concentration parcels; the log of the concentration distribution becomes a uniform distribution. Consequently, I use the median rather than the mean as a bulk statistic for these populations.
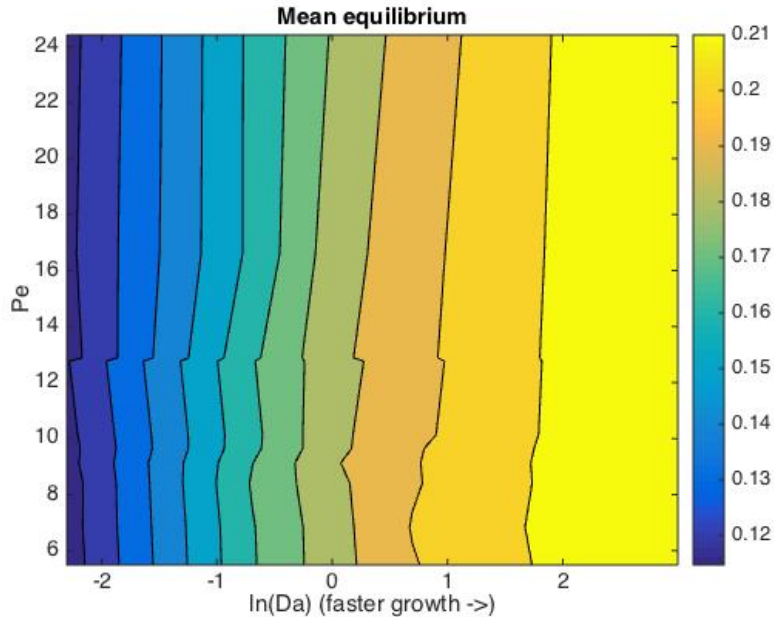

Figure 14: Median concentration of plankton as a function of both growth rate and Peclet number

Figure 14 shows the median phytoplankton concentration after equilibrium as a

function of the growth rate and Peclet number. While the concentration depends on the growth rate, it does not depend strongly on the Peclet number. This indicates that transport of water parcels rather than exchange of material between parcels is a more important factor controlling the population dynamics. Reducing γ, the growth rate of the plankton relative to mixing speed, reduces the equilibrium concentration of the plankton. The reduced concentration can be thought of as an effective carrying capacity due to strong stirring.

5.1.1 Analytic results for dependence on time scale

The finding that the equilibrium plankton concentration with relatively fast growth rates is higher than equilibrium plankton concentration with slow growth rates can be predicted from the spatially dependent logistic growth equation. The effects of stirring disappear with fast growth rate, so the equilibrium population is the arithmetic spatial average of carrying capacity. With slow growth rate relative to stirring rate the effective carrying capacity an individual parcel containing phytoplankton is exposed to many carrying capacities during the time scale of its reaction. So the equilibrium population level would be a spatial average of the carrying capacity. I set $\frac{dP}{dt} = 0$ to find the equilibrium value, which satisfies:

$$\gamma P \left(1 - P \left\langle \frac{1}{K(\mathbf{r})} \right\rangle \right) = 0 \tag{28}$$

Then, $P = \langle \frac{1}{K} \rangle^{-1}$, which is the harmonic mean of the carrying capacity, as derived in [30]. Thus, the equilibrium concentration depends on the time scale of the reaction.

5.1.2 Out of equilibrium population dynamics

With a constant stirring rate, slower growth rates also result in oscillations after an initial transient phase. Both the period and the amplitude of these oscillations depend on the time scale of the biological reaction (figure 15). The period and amplitude of the oscillations and the effective carrying capacity might also be expected to depend on the relationship between the spatial distribution of the carrying capacity in relation to the advection function. The oscillations are likely due to the historic dependence of the plankton concentration on both past light levels and past population concentrations. A population can be transported to a location where it is above the local carrying capacity, resulting in a population crash. Indeed, examining the concentration of plankton in a single water parcel over time shows that the bulk fluctuations in plankton concentration are caused by taking the average of many out of equilibrium oscillating populations (figure 16).

Although the mean equilibrium value of the population does not noticeably depend on the Peclet number, the Peclet number could still influence the population dynamics given that each water parcel is fluctuating out of equilibrium (figure 16). In particular, I find that the correlation between light history and abundance history depends on both the Peclet number and the growth rate. Calculating the cross-correlation between the time series of light levels and time series of plankton
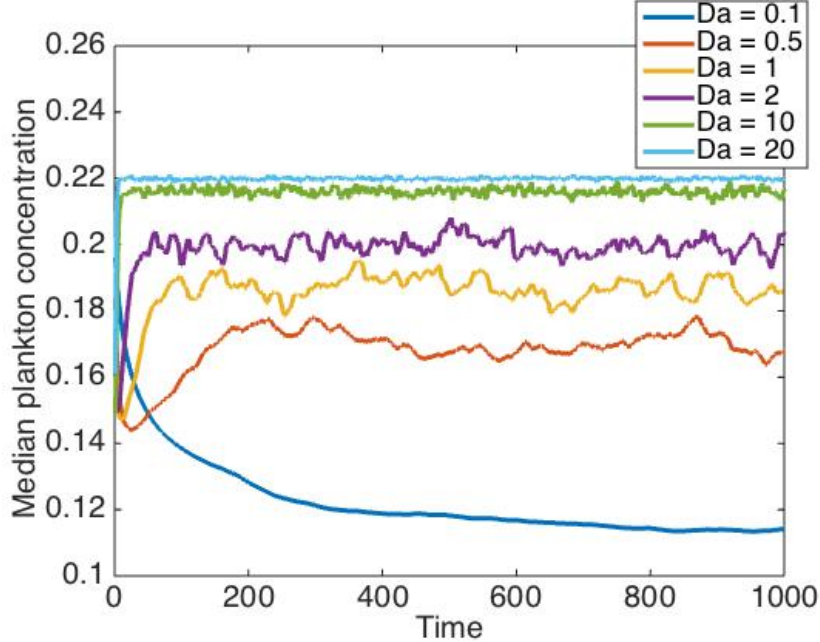
Figure 15: Mean concentration of plankton with different growth rates. The arithmetic mean carrying capacity for this population is 0.22. The harmonic mean carrying capacity for this population is 0.04.

concentration for each water parcel as it moves in the turbulent flow reveals that population abundance is most correlated with light levels 0-8 time steps after encountering that light level. The lag is greater with slower growth at larger Pe (figure 17).

Increasing the Peclet number results in less exchange of material between neighboring water parcels and thus higher variance in phytoplankton concentration at a particular depth, particularly in shallower water (figure 18 left). Reaction timescale is linked to diffusion timescale through the advective timescale. To be concrete, the ratio of diffusive timescale to reactive timescale is $Da \cdot Pe$. In this case, it seems that the smoothing effect of larger diffusion increases the rate at which populations reach equilibrium with the local environment.

Mean population variance also depends on both Pe and on Da. With logistic reactions, variance peaks at shallow depths (figure 18). Concentration variance peaks at intermediate depths for non-reacting tracers (figure 6). The difference is likely due to the higher concentrations at shallow depths in the cases with light-dependent growth. At smaller values of Da, the concentration variance peak shifts to intermediate depths, as would be expected for the non-reacting limit. Due to the smoothing effect of diffusion, the peak concentration variance is higher for larger Pe. Concentration variance also has the largest peak concentration variance when Da is order 1. At higher and lower Da values, concentration variance is lower. Da order 1 means that biological reaction timescales and turbulence timescales are around the same. These results demonstrate a case in which spatial heterogeneity emerges from turbulence
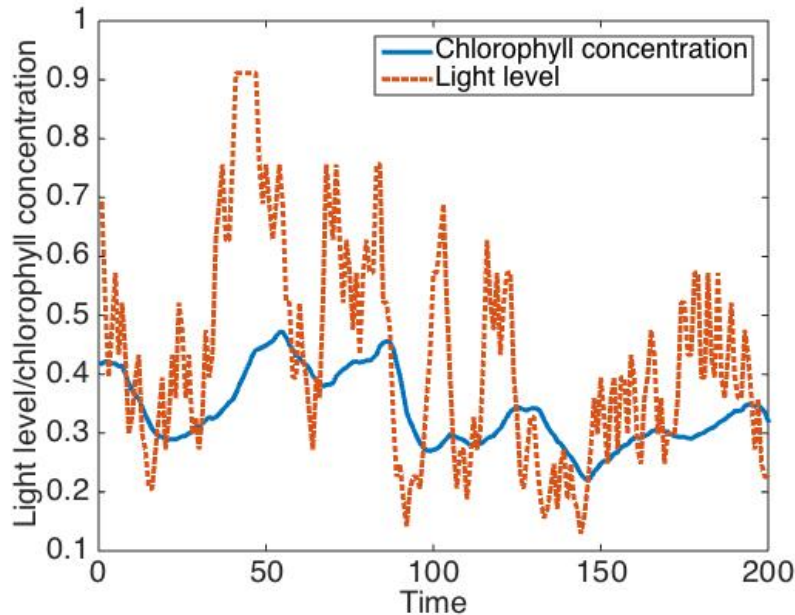
Figure 16: Red dashed: Light history of a single water parcel. Blue solid: Concentration of plankton in the water parcel. The population had $Da = 1$ and diffusion was a four-point smoother (b = 0).

and growth at the same timescale, rather than stirring creating inhomogeneities by stretching a localized bloom.

5.1.3 Perturbation analysis: traveling wave solutions

Analytically, diffusion does have an effect on the progress of a reaction, even reactions are spatially homogenous. In this section, I derive a result that provides theoretical support for the result presented in the last section with regards to the lag in correlation between light levels and population abundances (figure 17). With a particular initial condition, a traveling wave solution can be found to the non-linear reaction-advection-diffusion system with a logistic reaction term. Adding a small diffusion term to equation 19 introduces a spatial dependence that results in coupling the concentration of a parcel to the concentration of neighboring parcels. The small diffusion term represents a large Peclet number. I show that the traveling wave velocity depends on the Peclet number in a way that is consistent with the idea that, for large Peclet number, there is greater lag at larger Peclet number. This result is presented in equation 38, and derived below.

$$\frac{\partial N}{\partial t} + U\frac{\partial N}{\partial x} - Pe^{-1}\frac{\partial^2 N}{\partial x^2} = N(1 - N) \tag{29}$$

In this equation, U is a constant velocity. A change of coordinates to solve the equation in the moving frame reduces this to a reaction-diffusion problem. Use the
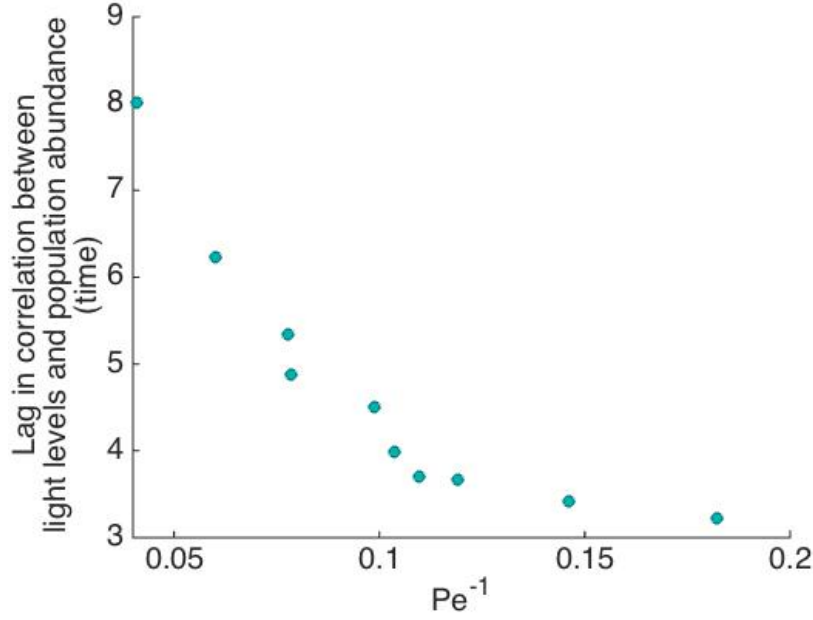
30

Figure 17: Lag in correlation between light levels and population concentration, calculated from time series of both concentration and light levels for each water parcel along a Lagrangian trajectory. Pe is the Peclet number for the case with no reactions.

coordinate change $l = x - Ut$ and $t = \tau$ and rewrite equation 29 as

$$
\begin{aligned}
-U\frac{\partial N}{\partial l} + \frac{\partial N}{\partial \tau} + U\frac{\partial N}{\partial l} - Pe^{-1}\frac{\partial^2 N}{\partial l^2} &= N(1-N) \\
\frac{\partial N}{\partial \tau} - Pe^{-1}\frac{\partial^2 N}{\partial l^2} &= N(1-N)
\end{aligned}
\tag{30}
$$

The reaction term $(f(N) = N(1-N))$ is smooth for $0 \leq N \leq 1$ and positive on that interval, except that $f(0) = f(1) = 0$. The steady state at $N = 0$ is unstable while the steady state at $N = 1$ is stable. These are general conditions on the reaction term in the Fisher-KPP equation and control the initial condition for a traveling wave solution. The initial condition, $N_0 = g(l, 0)$ is constrained such that $0 < g(l) < 1$ and $g(l) \to 1$ as $l \to -\infty$, $g(l) \to 0$ as $l \to +\infty$. The initial condition connects the two steady states of the reaction term. I choose

$$
g(l) = \frac{1}{1 + e^{\lambda l}}
\tag{31}
$$

and find a traveling wave solution to equation 30 on an infinite line.

The small diffusion term introduces a second time scale into the logistic growth reaction term. Using a multiple scales expansion,

$$
\begin{aligned}
\tau_1 &= \tau = t, \ \tau_2 = Pe^{-1}\tau \\
N &\sim N_0 + Pe^{-1}N_1 + ... \\
(\partial_{\tau_1} + Pe^{-1}\partial_{\tau_2})N &= Pe^{-1}\partial_{ll}N + N(1-N)
\end{aligned}
$$

The order 1 solution is

$$
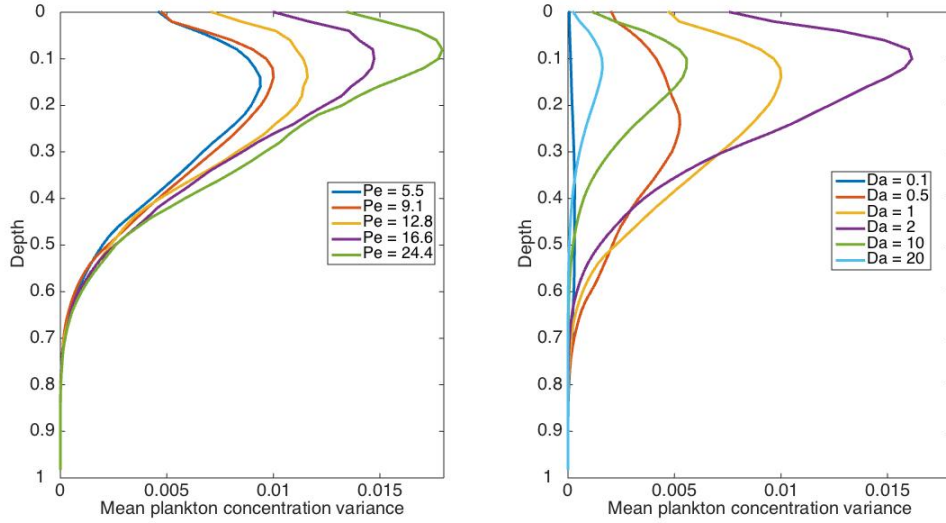\partial_{\tau_1} N_0 = N_0(1 - N_0)
$$

31

Figure 18: **Left**: Vertical profiles of phytoplankton concentration variance with $Da = 1$ for different Peclet numbers. **Right**: Vertical profiles of phytoplankton concentration variance with $Pe = 9.1$ for different growth rates.

with initial condition

$$N_0(l, 0, 0) = g(l)$$

this equation can be solved using separation of variables

$$\int_{1/2}^{c_0} \frac{ds}{s(1-s)} = \tau_1 + \Theta(l, \tau_2) \tag{32}$$

with initial condition

$$\int_{1/2}^{g(l)} \frac{ds}{s(1-s)} = \Theta(l, 0)$$

Equation 32 can be rewritten as an implicit solution

$$N_0 = n_0(\tau_1 + \Theta(x, \tau_2)) \tag{33}$$

where $n_0(r)$ satisfies $\int_{1/2}^{n_0} \frac{ds}{s(1-s)} = r$, so

$$n_0(r) = \frac{1}{1 + e^{-r}}$$

The order Pe^{-1} equation is

$$\partial_{\tau_1} N_1 = \partial_{ll} N_0 + N_1(1 - 2N_0) - \partial_{\tau_2} N_0$$

Plugging in equation 33,

$$\partial_{\tau_1} N_1 = N_1(1 - 2N_0) + N_0(1 - N_0)[\Theta_{ll} - \Theta_{\tau_2} + (1 - 2N_0)\Theta_l^2]$$

and integrating yields an expression for N_1 in terms of N_0 and Θ.

$$u_1 = N_0(1 - N_0)[A(l, \tau_2) + (\tau_1 + \Theta)(\Theta_{ll} - \Theta_{\tau_2}) + \Theta_l^2 \ln(N_0(1 - N_0))] \qquad (34)$$

As $\tau_1 + \Theta \to -\infty$, $N_0 \to 0$ and the logarithmic term in 34 produces a secular term $(\ln(N_0(1 - N_0)) \sim \tau_1 + \Theta)$. Therefore, require that

$$\Theta_{ll} - \Theta_{\tau_2} + \Theta_l^2 = 0 \qquad (35)$$

This equation can be solved using the change of variables $w(l, \tau_2) = e^{\Theta(l,\tau_2)}$. Equation 49 then reduces to a linear diffusion equation with space and time on the same scale.

$$w_{ll} = w_{\tau_2}$$

where

$$w(l, \tau_2) = e^{-\lambda l}\sqrt{\frac{\tau_2}{\pi}}\int_{-\infty}^{\infty} e^{\tau_2 s(s-2\lambda)}ds = e^{-\lambda l + \lambda^2 \tau_2}$$

The asymptotic approximation to equation 30 is then

$$N \sim \frac{1}{1 + e^{\lambda l - (1 + \lambda^2 Pe^{-1})\tau}} \qquad (36)$$

and the asymptotic approximation for the full reaction-advection-diffusion system (equation 29) is

$$N \sim \frac{1}{1 + e^{\lambda(x - Ut) - (1 + \lambda^2 Pe^{-1})t}} \qquad (37)$$

The traveling wave velocity is $v(l) \sim \frac{1 + \lambda^2 Pe^{-1}}{\lambda}$. The expected lag in the propagation of a traveling wave depends on the length scale of the problem.

$$\text{lag} \approx \frac{L}{v(l)} \sim \frac{\lambda L}{1 + \lambda^2 Pe^{-1}} \qquad (38)$$

Although the numerical simulations are done on a 2D periodic domain rather than an infinite line and with spatially dependent advection terms, the existence of a traveling wave solution that depends on Pe for this type of equation suggests one way in which diffusion adds spatial heterogeneity to an otherwise spatially uniform reaction system.

5.2 Spatial scale of equilibrium dynamics

In this section, I systematically vary the spatial field of the carrying capacity. Again, with light as the limiting resource, a faster rate of decrease of light intensity within the lattice used in the simulation could mean that plankton are being mixed to a greater depth (an assumption on both the speed of mixing and the depth of the actively mixing layer) or represent seasonal or spatial variation in light penetration. A survey of light penetration depth found that the 1% light level is around 5 meters in coastal areas and 50 meters in the open ocean [11]. Normalizing using a 50 meter

mixed layer depth, this corresponds to values of λ, as defined in equation 25, of 0.09-0.9 in non-dimensional form.

As in section 3, a faster mixing rate causes a lower spatially averaged population at equilibrium (figure 19, point D). The harmonic mean, as derived in the last section (equation 28), is the effective carrying capacity of the slow growth limit. Figure 19 shows the shape of the dependence of effective carrying capacity on the spatial and temporal parameters used in the advection-reaction-diffusion system.
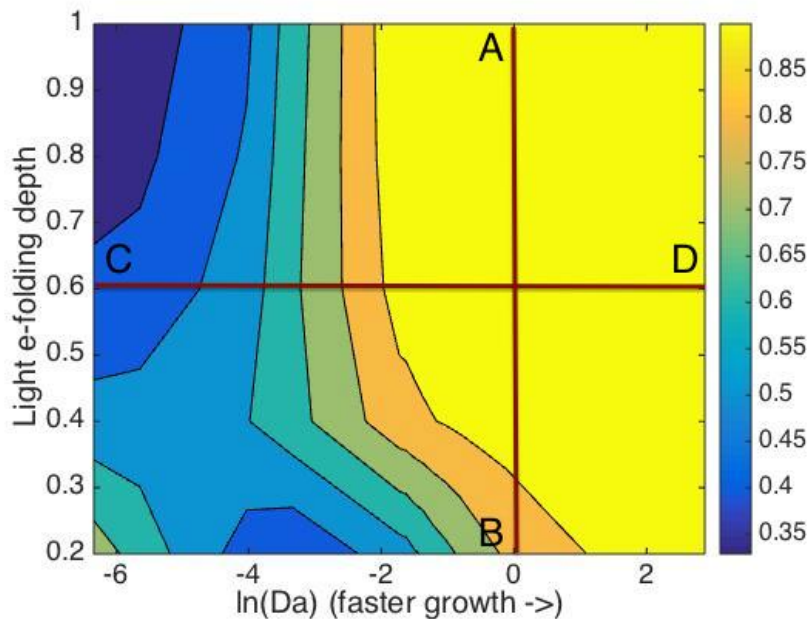

Figure 19: Median concentration of plankton with advection and diffusion normalized by mean carrying capacity $K(\mathbf{r})$. The e-folding depth of light, λ, is plotted on the vertical axis (equation 25). The horizontal axis shows the ratio of growth to stirring, Da, on a log scale. Slower growth relative to stirring is on the right hand side of the graph. The red lines show the parameter combinations used in the depth profiles in figure 20

The modeled gradients in Da and in light penetration can be used to discuss the critical turbulence hypothesis, which posits that the rate of mixing determines bloom formation, in relation to the critical depth hypothesis, which posits that the depth of mixing determines bloom formation. In figure 19, line AB corresponds to the mixed layer depth variation that the critical depth hypothesis posits as key to bloom dynamics. Figure 19 line CD corresponds to the stirring rate variability that the critical turbulence hypothesis claims controls bloom dynamics. Along line AB, for a given Da, a smaller e-folding depth will result in more extreme variation in light concentrations experienced by a particular population of phytoplankton. Plankton are also exposed to lower spatially averaged light concentrations (spatial mean and spatial harmonic mean concentrations). Thus, with shallower light penetration (figure 19, point B), mean plankton concentrations will be lower.

Phytoplankton in the regime with low light penetration relative to mixing depth will also be farthest from equilibrium. For example, in figure 20a, the curve $\lambda = 1$ is the closest to vertical, indicating that for a given light level, local populations are on average near or at their concentration limit for that particular light level. Populations tend to be below the expected concentration at the top, where light levels are high, and above the expected concentration at the bottom, where light levels are low. This is particularly true for the case where $\lambda = 0.2$, the shallowest light e-folding depth used. More extreme variation in light availability results in a situation in which phytoplankton concentrations, considered in the whole frame, are farther from equilibrium.
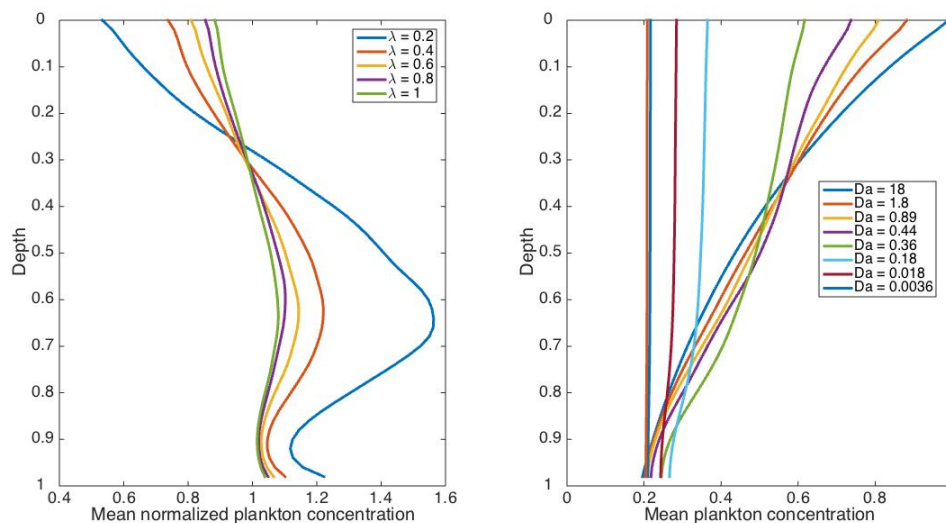

Figure 20: **a**: Vertical profiles of phytoplankton concentration with $Da = 1$ for different light e-folding depths. Mean phytoplankton concentration at each depth is normalized by $N(z)$ as written in equation 25 for each value of λ. The vertical red line in figure 19 shows overall average for the parameters used for this figure. **b**: Vertical profiles of phytoplankton concentration with $\lambda = 0.6$ for different Da. The horizontal red line in figure 19 shows overall average for the parameters used for this figure.

Along the line CD, for a given light e-folding depth, slower biological growth relative to mixing produces a more uniform vertical distribution of phytoplankton. However, for faster biological growth relative to mixing, the vertical profile of plankton concentration nearly matches the exponential decay profile of light availability with depth (figure 20b). Sverdrup's critical depth hypothesis assumes uniform distribution of phytoplankton. The result presented here demonstrate that this assumption may imply additional assumptions about the growth rate of phytoplankton, namely that growth rate is low compared to the rate of stirring in the system. In the critical turbulence hypothesis, the exact ratio of growth to stirring timescales (Da) required to maintain a uniform distribution of phytoplankton with depth depends on the light e-folding depth [16]. These results help to constrain exactly which values of Da should

be considered "slow" and "fast" when referring to the critical turbulence hypothesis when plankton grow non-linearly. Parameters for which the plankton concentration is uniform with depth should be characterized as fast stirring/slow growth regimes in which the critical depth criterion might be expected to be most relevant. In slow stirring/fast growth regimes, interaction between turbulent and biological timescales is likely more important. For the realistic case of intermediate light penetration (shown in figure 20a), cases with Da order 1 fall into a slow stirring regime, where the critical turbulence hypothesis is most relevant.

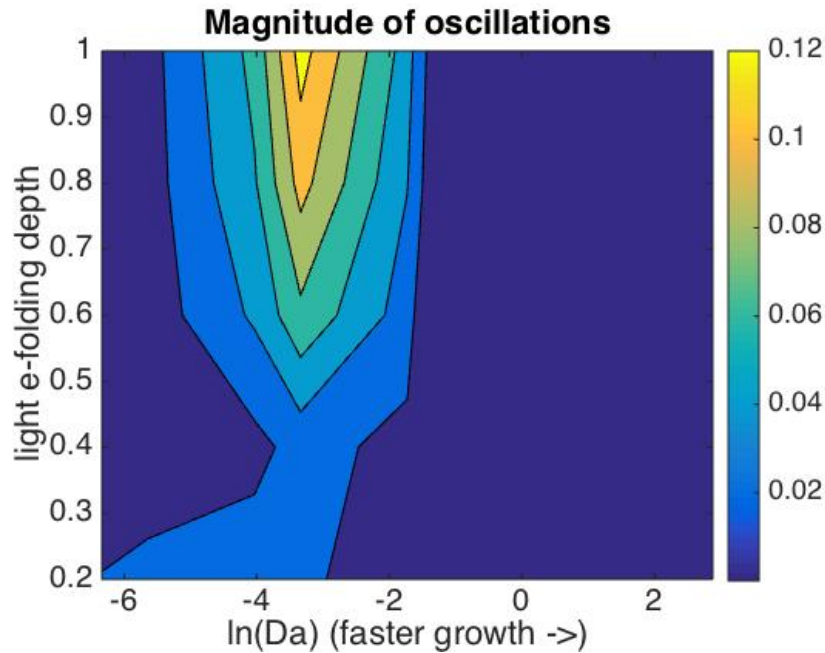Bulk and single particle oscillations are not only due to the ratio between

Figure 21: Difference between the upper and lower quartile values of the phytoplankton concentration once it has reached equilibrium, normalized by carrying capacity. The light e-folding depth, λ, is plotted on the vertical axis. Deeper light penetration is at the bottom of the graph. The horizontal axis shows the natural log of the Damkohler number, Da. Faster stirring relative to biological reaction rate is on the left hand side of the graph.

biological and turbulent timescales (figures 15 and 16), but also the degree of spatial heterogeneity. Figure 21 shows that for a shallower light e-folding depth, the case in which the vertical profile of plankton is most out of equilibrium, bulk oscillations are the greatest. In addition, as previously discussed, oscillations are greatest at intermediate growth rates. Again, examining figure 20a this is the case in which the system is farthest from the limits of either exponential decay in concentration with depth or uniform distribution with depth.

5.3   Cubic reaction terms

While logistic growth is a common model for population dynamics, in this case it might not necessarily be the best choice for a model of population dynamics. Instead, a model in which local populations that reach too low concentrations have the possibility of going extinct would better incorporate the effects of low light conditions on a phytoplankton population. This can be accomplished by using a cubic reaction model.

$$F(P; \mathbf{r}) = \gamma P\left(1 - \frac{P}{K(\mathbf{r})}\right)(P - a) \tag{39}$$

where a is less than $K(\mathbf{r})$. By introducing this additional term, zero becomes a stable steady state. The value a is an unstable steady state. Population concentrations below a will decrease while population concentrations above a will increase to the stable steady state $K(\mathbf{r})$. In the reaction-advection-diffusion system, a local population can recover from extinction and increase above a by exchanging material with a neighboring water parcel. Similarly, a population can decrease below a and towards extinction through exchange of material with neighboring parcels.

Again, the Damkohler number is defined as a time- and space-invariant quantity

$$Da = \left\langle \frac{\bar{u}}{L} \right\rangle \gamma \tag{40}$$

Where γ is the exponential growth rate in equation 26, the over bar represents the time mean and the angle brackets represent the spatial mean.

The cubic growth model must be used with much more care than the logistic growth model. One caveat is that populations with concentrations below a will go to zero faster when exposed to higher carrying capacities ($K(\mathbf{r})$) and will require a perturbation, such as diffusion of material from a neighboring water parcel, to increase above a. Consequently, this model is more sensitive to initial conditions than the logistic model. An initial population with concentration below a will go to the zero steady while one above a will go to the carrying capacity. Without some forcing, such as diffusion, to push a population above or below a, this parameter becomes and upper or lower bound, depending on the initial condition. In addition, the cubic model is only reasonable for small a relative to the expected value of $K(\mathbf{r})$. In the following simulations I use $a = 0.05$ and $a = 0$. With $\lambda = 0.01$, the average value of $K(\mathbf{r})$ is 0.791 and the minimum is 0.0105. If a is greater than $K(\mathbf{r})$, then a becomes the stable steady state and the carrying capacity $K(\mathbf{r})$ is unstable.

5.3.1   Spatial distribution

Similarly to the logistic growth equation, average plankton concentration depends strongly on reaction rate. The concentration also depends on Pe for fast growth (figure 22). The average plankton concentrations change more rapidly when $Da \approx 1$ with a cubic reaction term. While different average biomass may be expected for different order reaction terms, this distribution of productivity change suggests that a different scaling of Da would be more appropriate for comparison. In section 5.2,
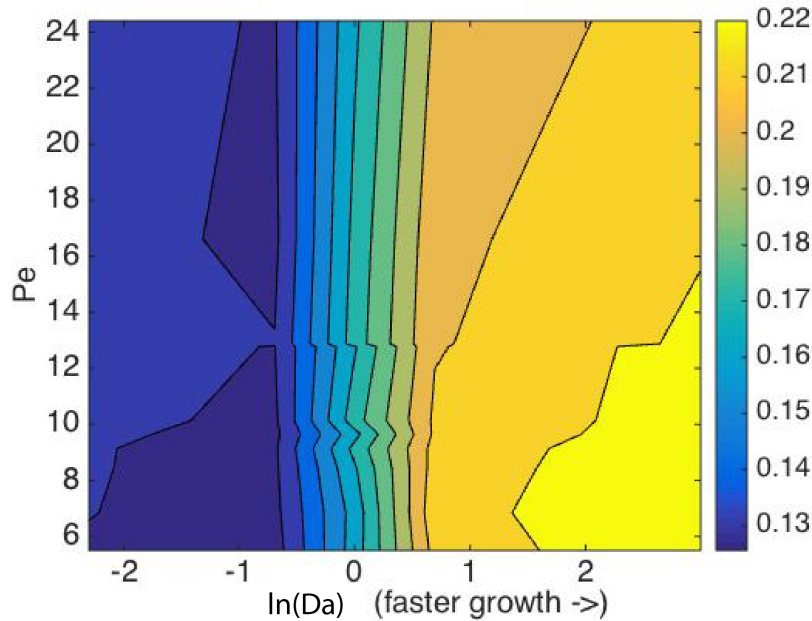
Figure 22: Median concentration of plankton as a function of both growth rate and Peclet number

I demonstrated that vertical distribution of average chlorophyll concentrations with depth are diagnostic of particular relationships between turbulence and reaction rate. Figure 23 shows that the depth distributions of plankton for a given value of Da are significantly different from those with forcing from a quadratic reaction term (figure 20), especially for intermediate growth rates. Based on this result, I suggest that Da should be parameterized differently with different order non-linear reactions.

I have made a substantial simplification by assuming that Da is constant through time, even with a saturating growth profile. With saturating growth, rate of accumulation of biomass depends on the population size. A more accurate Damkohler number for a reaction-advection diffusion system with an order n reaction term should be $Da \approx \frac{u}{L}\gamma(1 - \frac{P}{K})^{n-1}$. This definition of Da means that for a given vertical profile, Da would depend on the depth (since K depends on depth) as well as local plankton concentration. In other words, Da would vary quite substantially in space and time. Given that in this and in previous sections I have obtained useful results by using a constant Da, I propose that developing a value of Da that depends on just the reaction rate, γ, and the order of the reaction term, n, would be a useful contribution. It may also be interesting to develop a similar summary statistic that is a function of γ, n, and the light e-folding depth, λ.

5.3.2   Traveling wave solution for cubic reaction

Not only does the reaction-advection-diffusion system model with a cubic reaction term model some relevant properties of ecological populations that are left out in models of logistic growth, this system also has an exact traveling wave solution on
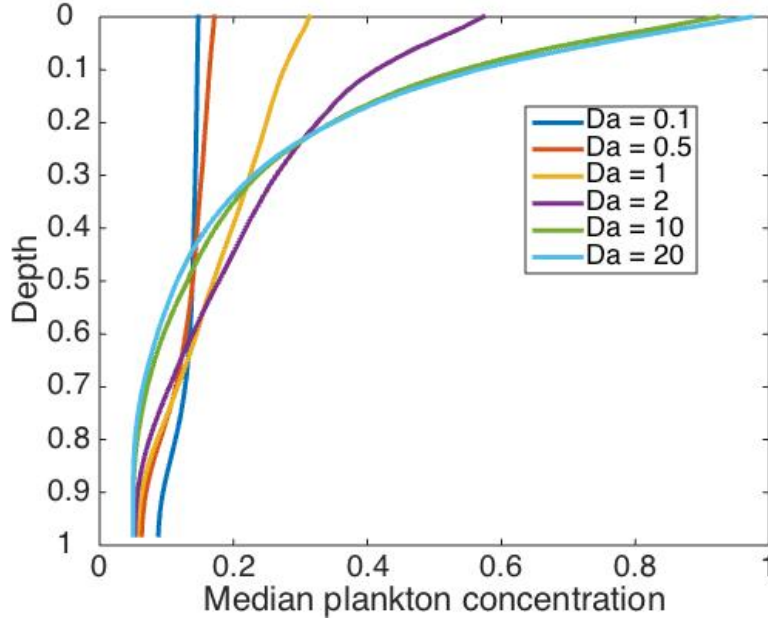
Figure 23: Average concentration of plankton as a function of depth with $Pe = 24$. Each curve has a different value of Da. The dark blue line $(Da = 0.1)$ is the case with the slowest reaction. The light blue line $(Da = 20)$ is the case with the fastest reaction.

the line.

$$\frac{\partial N}{\partial t} + U\frac{\partial N}{\partial x} + \frac{\partial^2 N}{\partial x^2} = N(N - a)(1 - N) \tag{41}$$

In this equation, U is a constant velocity. A change of coordinates to solve the equation in the moving frame reduces this to a reaction-diffusion problem. Use the coordinate change $l = x - Ut$ and $t = \tau$ and rewrite equation 29 as

$$
\begin{aligned}
-U\frac{\partial N}{\partial l} + \frac{\partial N}{\partial \tau} + U\frac{\partial N}{\partial l} + \frac{\partial^2 N}{\partial l^2} &= N(N - a)(1 - N) \\
\frac{\partial N}{\partial \tau} + \frac{\partial^2 N}{\partial l^2} &= N(N - a)(1 - N)
\end{aligned}
\tag{42}
$$

Assume a traveling wave solution with velocity v and make the change of variables $\xi = l + v\tau$ to find this solution $N(l, \tau) = \phi(l + v\tau)$ and let ' denote differentiation with respect to ξ to obtain the second order equation

$$vN' = N'' + N(N - a)(1 - N) \tag{43}$$

Substitute $N' = g(N)$.

$$vg(N) = g'(N)g(N) + N(N - a)(1 - N) \tag{44}$$

Make the Ansatz $g(N) = bN(1 - N)$. This is a good Ansatz because:

- $g(0) = g(1) = 0$

39

- The Ansatz is smooth and positive for $0 < N < 1$

- The two terms on the right hand side will be the same order. If $\mathcal{O}(g(N)) = 2$, $\mathcal{O}(g'(N)g(N)) = 1 + 2 = 3$, and $\mathcal{O}(N(N - a)(1 - N)) = 3$

Substituting in $g(N)$

$$vbN(1 - N) = b(1 - 2N)bN(1 - N) + N(N - a)(1 - N)$$
$$vb - b^2 + a = N(1 - 2b^2) \tag{45}$$

This equation is satisfied for all $N \in \mathbb{R}$ if and only if

$$1 - 2b^2 = 0 \implies b = \frac{1}{\sqrt{2}} \tag{46}$$

and if and only if the velocity is specified by the parameter a as follows

$$vb - b^2 + a = 0 \implies v = \frac{b^2 - a}{b} = \frac{1}{\sqrt{2}}(1 - 2a) \tag{47}$$

Finally, solve the equation $g(N) = N' = \frac{1}{\sqrt{2}}N(1 - N)$ to obtain

$$N(\xi) = \frac{e^{\xi/\sqrt{2}}}{N_1 + e^{\xi/\sqrt{2}}} \tag{48}$$

Assume $N(0) = \frac{1}{2} \implies N_1 = 1$.

$$N(\xi) = \frac{e^{\xi/\sqrt{2}}}{1 + e^{\xi/\sqrt{2}}} \tag{49}$$

5.3.3 Form of background heterogeneity

In section 4, I concluded using numerical simulations that spatially variable forcing is required to generate patchiness in a reaction-advection-diffusion system with a single plankton population and continuous growth. In this paper, I have chosen to investigate the impact of light availability on a bloom. While light availability is typically modeled as an exponential decay, as it is in this study, factors such as suspended particles and self-shading by a bloom could be meaningfully incorporated into models of bloom formation by altering this assumption. Many modeling studies have used step functions to model light availability in an analytically tractable fashion [16]. In the two dimensional model used in the numerical simulations in this paper could be reasonably approximated as one dimensional trajectories with a highly variable carrying capacity (figure 16). Although each are meaningful assumptions, the shape of light availability could affect the propagation of a bloom. In this section, I find an asymptotic solution to a general reaction-advection-diffusion system with a small spatially inhomogeneous reaction term and then investigate the way in which the propagation speed of the traveling wave solution depends on the shape of the spatially inhomogeneous function in the reaction term. Although I am currently

investigating a one-species model, propagation speed of a traveling wave would have important implications for competition between species, especially if the species have different parts of a spatial domain in which they grow fastest. In the single species scenario, traveling wave propagation speed could have implications for the likelihood of a bloom when resources are temporally heterogenous. One might ask if a bloom can occur before conditions change to be less advantageous to the bloom-forming population.

In the work below, I use an asymptotic expansion to investigate the effects of the form of a carrying capacity curve on bloom propagation. The existence of an exact solution for a traveling wave on the line for a cubic reaction term simplifies this calculation because diffusion and reaction are assumed to occur on the same timescale for the exact solution, so even with the assumption that the spatially varying carrying capacity is a small parameter, this asymptotic expansion only requires two timescales. After deriving a general equation for bloom propagation with spatially variable carrying capacity (equation 56), I plot the solutions for the example case of exponential decay of light with depth.

Modify equation 43 to have a general spatially varying carrying capacity and substitute $v = -v$

$$vc' = c'' + c((c-a)(1-c) + \epsilon K(x)) = c'' + c((c-a)(1-c) + \epsilon K(\xi + v\tau)) \quad (50)$$

Solve this equation by finding an asymptotic solution of the form

$$c = c_0 + \epsilon c_1 + \dots \quad (51)$$

The solution c_0 to the $\mathcal{O}(1)$ problem is the same as the solution given in equation 49. $c_0(\xi) = \frac{e^{\xi/\sqrt{2}}}{1+e^{\xi/\sqrt{2}}}$. The $\mathcal{O}(\epsilon)$ problem is

$$\partial_t c_1 + vc_1' = c_1'' + c_1(-3c_0^2 + 2(a+1)c_0 - a) + K(\xi + v\tau)c_0 \quad (52)$$

Find an approximation to equation 52 by decomposing $c_1(\xi, \tau)$ as

$$c_1(\xi, \tau) = p(\tau)c_0'(\xi) + \tilde{c}_1(\xi, \tau)$$

Where the first term on the right hand side represents a position change of the traveling wave and the second term represents a change in the shape of the traveling wave front. Rewriting equation 52 as

$$\partial_\tau c_1 = Lc_1 + h(\xi, \tau)$$

where L is an operator containing all of the linear terms in equation 52 and h is the higher order corrections. Equate the two formulations of $\partial_\tau c_1$ to obtain the equation

$$\dot{p}c_0' + \partial_\tau \tilde{c}_1 = pLc_0' + L\tilde{c}_1 + h(\xi, \tau) = L\tilde{c}_1 + h(\xi, \tau) \quad (53)$$

Assume that the two terms containing $\tilde{c}_0$ are equal by choosing a particular $\tilde{c}_0$ and a projection $w_1(\xi)$ such that $L^*w_1(\xi) = 0$. Solve the equation

$$(\partial_\xi^2 + v\partial_\xi + f'(c_0))w_1(\xi) = 0 \quad (54)$$

Assume a solution of the form $w_1(\xi) = e^{b\xi}c_0'(\xi)$ and plug this assumption into equation 54. Solve for b.

$$((b+\partial_\xi)^2 + v(b+\partial_x i))e^{b\xi}c_0' = (\partial_\xi^2 - v\partial_\xi)e^{b\xi}c_0'$$
$$b^2 + 2b\partial_\xi + \partial_\xi^2 + vb + v\partial_\xi = \partial_\xi^2 - v\partial_\xi$$
$$(b+v)(b+2\partial_\xi) = 0$$
$$\implies b = -v$$

For traveling wave velocity v, as defined in equation 47.

$$w_1(\xi) = \frac{1}{\sqrt{2}}e^{\left(\frac{1}{\sqrt{2}}(1-2a)\right)\xi}\frac{e^{\xi/\sqrt{2}}}{(1+e^{\xi/\sqrt{2}})^2} \tag{55}$$

Use the projection $w_1(\xi)$ to integrate 53.

$$\int_{-\infty}^{\infty} w_1(\xi)(\dot{p}c_0' + \partial_t\tilde{c}_1)d\xi = \int_{-\infty}^{\infty} w_1(\xi)(L\tilde{c}_1 + h(\xi,t))d\xi$$

By the assumption, the $\tilde{c}_1$ terms drop out and $K(\xi+v\tau) = h(\xi,t)$, leaving the integral

$$\dot{p}(\tau)\int_{-\infty}^{\infty} w_1(\xi)c_0'(\xi)d\xi = \int_{-\infty}^{\infty} w_1(\xi)K(\xi+v\tau)c_0(\xi)d\xi \tag{56}$$

Solve for $\dot{p}(\tau)$ using numerical integration for different functions $K(\xi - v\tau)$.

Exponential decay
Assume a profile of the form

$$K(x) = e^{-0.01x} \implies K(\xi + v\tau) = e^{-0.01(\xi+v\tau)}$$

$$\dot{p}(t) = \frac{\int_{-\infty}^{\infty} w_1(\xi)e^{-0.01(\xi+vt)}c_0(\xi)d\xi}{\int_{-\infty}^{\infty} w_1(\xi)c_0'(\xi)d\xi} = 1.129e^{-0.00636\tau} \tag{57}$$

Assuming $a = 0.05$, as in the numerical simulations, and integrating equation 57 in τ, the asymptotic expansion (equation 51) for a wave traveling down an exponential decay in carrying capacity (from high to low carrying capacity) is

$$c(l,\tau) = \frac{e^{(l-0.636\tau)/\sqrt{2}}}{1 + e^{(l-0.636\tau)/\sqrt{2}}} + \epsilon(-177.422e^{-0.00636396\tau} + 177.422)\frac{e^{(l-0.636\tau)/\sqrt{2}}}{\sqrt{2}(1 + e^{(l-0.636\tau)/\sqrt{2}})^2} \tag{58}$$

This solution represents a subtle slowing down when a localized population expands over an area with an exponential decay in resource availability, as opposed to uniform resource availability (figure 24).
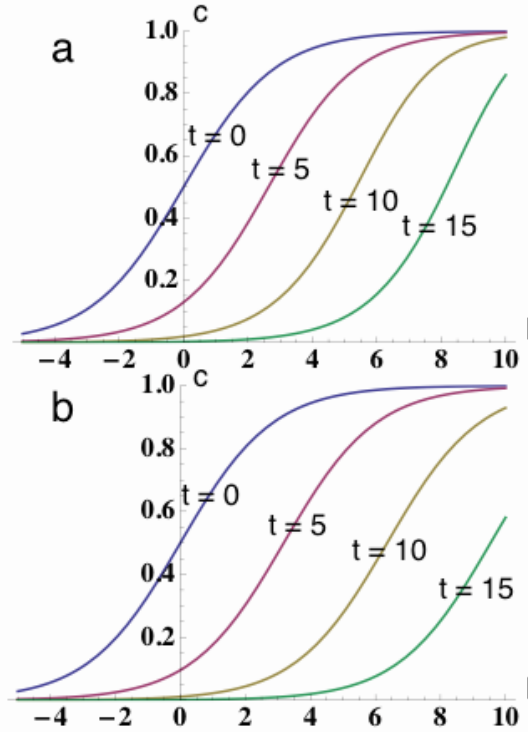
Figure 24: Traveling wave solution to a reaction-advection-diffusion system with **a** uniform carrying capacity ($K(x) = $ constant) and **b** exponentially decaying carrying capacity ($K(x) = \exp(-\lambda x)$) (equation 58) with $\epsilon = 0.1$.

5.4 Discussion

I have shown that not only does the depth of light penetration affect phytoplankton population dynamics, but also that the relative timescale of biological growth and advective transport are important determinants of phytoplankton population dynamics, in accordance with the predictions of the critical depth hypothesis and the critical turbulence hypothesis. I examined equilibrium solutions and found that due to the dependence of the plankton concentration on previous light levels, the whole system is out of equilibrium, particularly for $Da \sim \mathcal{O}(1)$, resulting in seemingly random fluctuations in mean concentration through time once at equilibrium. Through examining individual populations, it is clear that these fluctuations are an aggregation of many locally fluctuating populations. In the limiting cases of very slow and very fast growth relative to stirring, the average plankton concentration goes to a value determined by light availability in the mixed layer. With $Da \sim \mathcal{O}(1)$, high variance emerges as a result of the interaction between stirring and growth.

Most studies of plankton bloom formation do not separate the effects of chaotic advection and diffusion. In a turbulent environment, local populations that are growing with either logistic or cubic reaction terms are out of equilibrium due to chaotic advection. In addition, they are linked to each other through historic dependence on the light levels experienced along a given trajectory and through diffusion of material

with neighboring parcels. Diffusion between neighboring water parcels can generate traveling waves that propagate across the whole domain. The speed of propagation of a traveling wave, which models the the spread of a localized bloom, depends on Pe, or the degree of turbulence and random swimming by plankton and on the assumed form of background heterogeneity. Assumptions about the degree of background heterogeneity and the form of that heterogeneity can affect the propagation of a bloom. In this work, the background heterogeneity is in the form of exponential decay with depth, which plankton sample non-uniformly due to chaotic advection. Diffusion and advection have different effects on the blooming plankton population and should be considered separately when discussing the factors that trigger bloom formation.

Finally, I discussed the summary statistics used in this work. In particular, I suggest that substantial simplifications in the form of biological reaction rate are reasonable such that plankton concentration is not necessary to include in Da even with non-linear reaction terms. However, the effective growth rate, γ, and the order of the reaction term, n, are necessary to incorporate in Da. In addition, since the interaction between turbulence and biological growth are strongly dependent on the degree of background heterogeneity, including the light e-folding depth, λ, in a summary statistic of the relationship between reaction and advection could be informative.

6   Predator-prey

The logistic growth model can be modified to account for predation while preserving the dependence of the reactions on light levels. This system of equations (59-61) uses the inhomogeneous carrying capacity presented in equation (25) and a Holling type II functional response (which is saturating) to transfer mass between the prey and the predator. Both prey (P, for phytoplankton) and predator (Z, for zooplankton) experience the same mixing and stirring (same velocity, same value of Pe). In this section, I use the fluid model with doubly periodic boundary conditions. Using the fluid model with closed top and bottom boundaries would give further information about the spatial distribution of phytoplankton and zooplankton [2, 40].

$$N(z) = e^{-\lambda z} \tag{59}$$

$$\frac{\partial P}{\partial t} + \mathbf{v} \cdot \nabla P = \gamma \left[P \left(1 - \frac{P}{N(z)} \right) - a \frac{PZ}{P+S} \right] + Pe^{-1} \nabla^2 P \tag{60}$$

$$\frac{\partial Z}{\partial t} + \mathbf{v} \cdot \nabla Z = \gamma \left[ea \frac{PZ}{P+S} - mZ \right] + Pe^{-1} \nabla^2 Z \tag{61}$$

Where Z is the zooplankton population, m is the natural mortality rate of zooplankton, e is the conversion efficiency of phytoplankton into energy for the zooplankton, and S parameterizes the functional response of the intake rate of the zooplankton to number of phytoplankton consumed.

Again, I use a simple formulation of the Damkohler number

$$Da = \left\langle \frac{\bar{u}}{L} \right\rangle \gamma \tag{62}$$

Where γ is the exponential growth rate in equation 26, the over bar represents the time mean and the angle brackets represent the spatial mean. I have not formulated an additional Damkohler number for zooplankton. Instead, I analyze only the phytoplankton population dynamics. Incorporating either linear or non-linear loss terms into a generalized time and space varying or time-and space-invariant Damkohler number may be required for some applications. However, as I show in the analysis below, even a Da statistic based on the exponential growth phase alone gives useful information about population dynamics.

6.1 Bifurcations and oscillatory dynamics

This two-dimensional non-linear system can result in oscillations for certain parameter combinations. A set of parameters that results in oscillations without mixing is shown in table 2.

Table 2: NPZ oscillatory model parameters

Parameter	Value
λ	0.06-0.1
γ	0.1-1
a	1.67
S	0.3
e	0.3
m	0.2

Strong stirring in a strongly non-uniform carrying capacity field can result in oscillator death, because the effective carrying capacity is reduced beyond the bifurcation point of the oscillatory system [30]. Oscillator death results from a Hopf bifurcation. The bifurcation curve can be predicted analytically for the case without stirring. In order to investigate the effects of stirring, I plotted time-series for a wide range of parameter values and classified the results as oscillatory if the result was clearly approaching a stable limit cycle and decaying (oscillator death) if the oscillations were decaying. Predictably, with a more homogenous medium, meaning slower rate of decay of the carrying capacity, stirring has a smaller effect and does not cause the system to pass a bifurcation point. For a given rate of decay of carrying capacity, though, stirring does affect the coupling of the oscillators (the two populations), with slow reaction rates decoupling oscillators when the carrying capacity is more inhomogeneous. The phase portrait is shown in figure (25). This result is analogous to a result obtained for chemical reactions in an oscillatory medium [31].

In order to find the bifurcation curve analytically, I assume that there is a constant steady state and analyze the linearized system. The Jacobian of the system of growth (reaction) functions in equations (60) and (61), assuming a spatially constant steady state, is given by

$$\begin{pmatrix} \gamma^{-1}[1 - \frac{2P}{K} - \frac{aSZ}{(P+S)^2}] & \gamma^{-1}[\frac{-aP}{P+S}] \\ \gamma^{-1}[\frac{-eaSZ}{(P+S)^2}] & \gamma^{-1}[\frac{-aeP}{P+S} - m] \end{pmatrix}$$
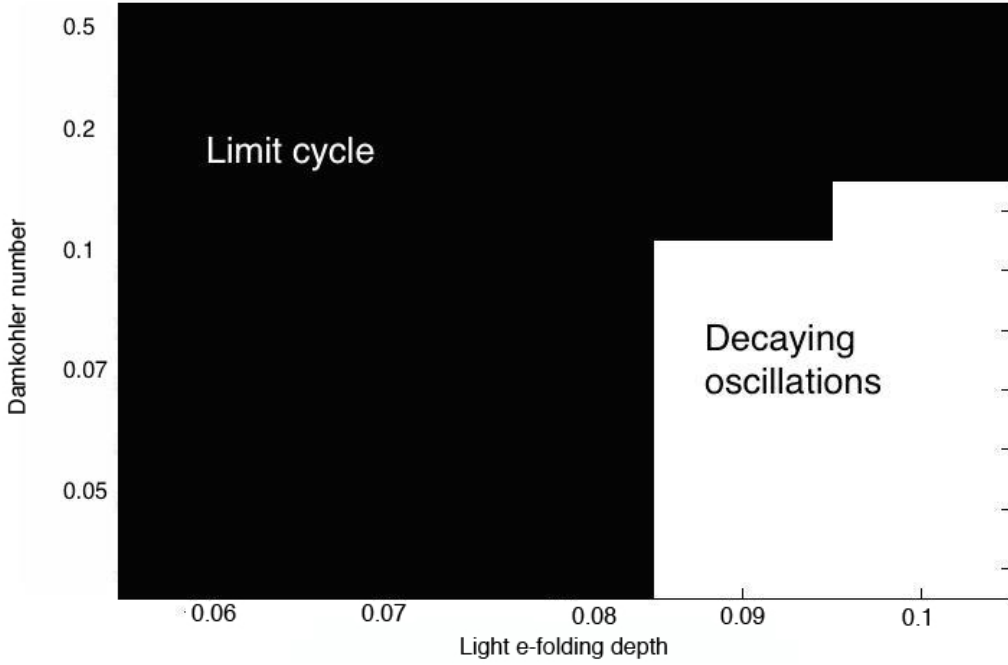
Figure 25: Phase diagram of the oscillatory system with exponentially decaying carrying capacity. The top left has higher reaction rates or lower stirring rates and a more homogenous carrying capacity. Parameter combinations in the black region result in stable limit cycles for both the zooplankton and phytoplankton in the steady state. Parameter combinations in the white region result in decaying oscillations for both the zooplankton and phytoplankton in the steady state.

The trace is given by

$$\tau = \gamma^{-1}[1 - \frac{2P}{K} - \frac{aSZ}{(P+S)^2} - \frac{aeP}{P+S} - m] \tag{63}$$

At a co-existence steady-state (P^*, Z^*), there exists a positive solution to

$$\gamma^{-1}[(1 - \frac{P^*}{K}) - a\frac{Z^*}{P^* + S}] = 0 \tag{64}$$

$$\gamma^{-1}[ea\frac{P^*}{P^* + S} - m] = 0 \tag{65}$$

Using equation (65) to simplify equation (63), I get

$$\tau = \gamma^{-1}[1 - \frac{2P^*}{K} - \frac{aSZ^*}{(P^* + S)^2}] \tag{66}$$

Then I rearrange equation (64) to become $1 - \frac{P}{K} = \frac{aZ}{P+S}$ and substitute into equation (66) and simplify to get

$$\tau = \gamma^{-1}[\frac{P^*}{K(P^* + S)}(K - S - 2P^*)] \tag{67}$$

46

The bifurcation curve is defined by the values of K, the bifurcation parameter in all simulations, for which the trace is zero. This can happen when $K = S$. The co-existence steady state is stable (decaying oscillations) when $K < S$, when $K > S$, a Hopf bifurcation and then a stable limit cycle is possible.

The effective carrying capacity can be calculated for each combination of λ and γ and a given S to determine if stable limit cycles are possible as long as P begins small and $\frac{dP}{dt} > 0$. For example, compare figure 25 to figure 19. Therefore, the ratio between the mixing rate and the reaction rate, γ, is a bifurcation parameter for this system. All simulations presented in figure 25 had spatially averaged carrying capacities above 0.6. Given S = 0.3, the value used for all simulations, none would have passed the bifurcation point without mixing.

6.2 Discussion

The set of results that investigate the predator-prey dynamics represented by a two dimensional non-linear system draw on principles of non-linear coupled oscillators. Combining the results from the logistic growth (phytoplankton and nutrients only) and the three dimensional system that had oscillations (nutrients, phytoplankton, and zooplankton) revealed that Da acts as a bifurcation parameter by modifying the effective carrying capacity of the system, which has carrying capacity as a bifurcation parameter in the non-turbulent case. With faster stirring, phytoplankton never have time to reach equilibrium, so the mean equilibrium population is below the arithmetic spatial average of carrying capacity. This link through plankton biomass between the dilution-recoupling hypothesis and the critical turbulence hypothesis suggests a that merging the two hypotheses could produce fruitful results in relation to the timing and dynamics of plankton blooms. Even the simple biological models used in section 5 when combined with spatially in homogenous growth and turbulence generate complicated dynamics. One question to be explored further is that of the interactions by zooplankton with spatially and temporally variable phytoplankton [31]. In this model, the phytoplankton are continuously out of equilibrium. Does suppression of phytoplankton by predation depend on the variance in phytoplankton concentration (figure 18)? Do bloom dynamics depend on the response time of zooplankton to changes in phytoplankton population [1, 15]? Answering these questions could provide a unified framework that incorporates top-down and bottom-up forcing of productivity during plankton blooms. Models such as those used in this work in which different forcing parameters can be separately investigated are particularly well-suited to developing such a framework.

7   Conclusion

The results presented in this paper have possible implications for global ocean productivity. One major challenge in observational biological oceanography is linking surface chlorophyll measurements from satellite ocean color sensors to mixed layer productivity. Turbulent mixing is one control on the depth distribution of a bloom.

If light is the limiting resource, slow mixing can create overall higher productivity, and particularly high productivity at the ocean surface, while fast mixing will generate more uniform productivity throughout the mixed layer. Including the effects of turbulent mixing on phytoplankton in biogeochemical models could improve the accuracy of models of bloom formation. Moreover, I have suggested integrating the effects of turbulence on both light exposure and predator exposure for a more thorough understanding of bottom up and top down drivers of bloom formation.

The modeling and analytic techniques developed and utilized in this paper could be used to analyze other theories of bloom formation and for an even more thorough description of the population dynamics that emerge from current hypotheses for bloom formation. The greatest strength of this method was the ability to separately examine each of the physical and biological drivers of bloom formation. In contrast to many previous studies of the critical depth and critical turbulence hypotheses, which used one dimensional simulations, I used a two dimensional domain for this simulation to demonstrate that chaotic advection and diffusion have different effects on bloom formation. This was possible because the exact-Lagrangian model I used can be parameterized to have a range of diffusion strengths, including no diffusion. More careful analysis of particular two dimensional flow features such as confluence and diffluence and of the degree of randomness in the flow field (represented by the non-dimensional t^*) could also yield insight into population dynamics.

8   Acknowledgements

References

[1] Edward R Abraham. The generation of plankton patchiness by turbulent stirring. *Nature*, 391(6667):577–580, 1998.

[2] Karl Banse. On the vertical distribution of zooplankton in the sea. *Progress in oceanography*, 2:53–125, 1964.

[3] Michael J Behrenfeld. Abandoning sverdrup's critical depth hypothesis on phytoplankton blooms. *Ecology*, 91(4):977–989, 2010.

[4] Michael J Behrenfeld and Emmanuel S Boss. Resurrecting the ecological under-pinnings of ocean plankton blooms. *Annual review of marine science*, 6:167–194, 2014.

[5] Michael J Behrenfeld, Scott C Doney, Ivan Lima, Emmanuel S Boss, and David A Siegel. Annual cycles of ecological disturbance and recovery underlying the sub-arctic atlantic spring plankton bloom. *Global biogeochemical cycles*, 27(2):526–540, 2013.

[6] Andrew F Bennett and Kenneth L Denman. Phytoplankton patchiness: infer-ences from particle statistics. *Journal of Marine Research*, 43(2):307–335, 1985.

[7] Philip W Boyd, Andrew J Watson, Cliff S Law, Edward R Abraham, Thomas Trull, Rob Murdoch, Dorothee CE Bakker, Andrew R Bowie, KO Buesseler, Hoe Chang, et al. A mesoscale phytoplankton bloom in the polar southern ocean stimulated by iron fertilization. *Nature*, 407(6805):695–702, 2000.

[8] George Leonard Clarke and Richard H Backus. Interrelations between the verti-cal migration of deep scattering layers, bioluminescence, and changes in daylight in the sea. *Bull. Inst. Oceanogr. Monaco*, 64(1318):1–36, 1964.

[9] John J. Cullen and Marlon R. Lewis. The kinetics of algal photoadaptation in the context of vertical mixing. *Journal of Plankton Research*, 10(5):1039–1063, 1988.

[10] EA D'Asaro, J Thomson, AY Shcherbina, RR Harcourt, MF Cronin, MA Hemer, and B Fox-Kemper. Quantifying upper ocean turbulence driven by surface waves. *Geophysical Research Letters*, 41(1):102–107, 2014.

[11] KL Denman and ANDA E Gargett. Time and space scales of vertical mixing and advection of phytoplankton in the upper ocean. *Limnology and Oceanography*, 28(5):801–815, 1983.

[12] Ute Ebert, Manuel Arrayás, Nico Temme, Ben Sommeijer, and Jef Huisman. Critical conditions for phytoplankton blooms. *Bulletin of mathematical biology*, 63(6):1095–1124, 2001.

[13] Richard W Eppley. Temperature and phytoplankton growth in the sea. *Fish. Bull*, 70(4):1063–1085, 1972.

[14] Geoffrey T Evans and John S Parslow. A model of annual plankton cycles. *Biological oceanography*, 3(3):327–347, 1985.

[15] Peter JS Franks. Phytoplankton blooms in a fluctuating environment: the roles of plankton response time scales and grazing. *Journal of plankton research*, 23(12):1433–1441, 2001.

49

[16] Sandip Ghosal and Shreyas Mandre. A simple model illustrating the role of turbulence on phytoplankton blooms. *Journal of mathematical biology*, 46(4):333–346, 2003.

[17] Jessica L Green, Alan Hastings, Peter Arzberger, Francisco J Ayala, Kathryn L Cottingham, Kim Cuddington, Frank Davis, Jennifer A Dunne, Marie-Josée Fortin, Leah Gerber, et al. Complexity in ecology and conservation: mathematical, statistical, and computational challenges. *BioScience*, 55(6):501–510, 2005.

[18] Stephen M Griffies, Michael Levy, Alistair J Adcroft, Gokhan Danabasoglu, Robert W Hallberg, Doub Jacobsen, William Large, and Todd Ringler. Theory and numerics of the community ocean vertical mixing (cvmix) project. 2013.

[19] Angelique C Haza, Tamay M Özgökmen, Annalisa Griffa, Zulema D Garraffo, and Leonid Piterbarg. Parameterization of particle transport at submesoscales in the gulf stream region using lagrangian subgridscale models. *Ocean Modelling*, 42:31–49, 2012.

[20] Jef Huisman, Paul van Oostveen, and Franz J Weissing. Critical depth and critical turbulence: two different mechanisms for the development of phytoplankton blooms. *Limnology and Oceanography*, 44(7):1781–1787, 1999.

[21] Roy Jonker and Anton Volgenant. A shortest augmenting path algorithm for dense and sparse linear assignment problems. *Computing*, 38(4):325–340, 1987.

[22] Ren-Chieh Lien, ERIC A D'ASARO, and Geoffrey T Dairiki. Lagrangian frequency spectra of vertical velocity and vorticity in high-reynolds-number oceanic turbulence. *Journal of Fluid Mechanics*, 362:177–198, 1998.

[23] Cristóbal López, Zoltán Neufeld, Emilio Hernández-García, and Peter H Haynes. Chaotic advection of reacting substances: Plankton dynamics on a meandering jet. *Physics and Chemistry of the Earth, Part B: Hydrology, Oceans and Atmosphere*, 26(4):313–317, 2001.

[24] Amala Mahadevan. Spatial heterogeneity and its relation to processes in the upper ocean. In *Ecosystem Function in Heterogeneous Landscapes*, pages 165–182. Springer, 2005.

[25] Amala Mahadevan, Eric D'Asaro, Craig Lee, and Mary Jane Perry. Eddy-driven stratification initiates north atlantic spring phytoplankton blooms. *Science*, 337(6090):54–58, 2012.

[26] Martin. The kaleidoscope ocean. *Philosophical Transactions of the Royal Society A*, 363(1873):2873–2890, 2005.

[27] Charles R McClain. A decade of satellite ocean color observations*. *Annual Review of Marine Science*, 1:19–42, 2009.

[28] Shakti N Menon and Georg A Gottwald. Bifurcations of flame filaments in chaotically mixed combustion reactions. *Physical Review E*, 75(1):016209, 2007.

[29] Zoltan Neufeld. Stirring effects in models of oceanic plankton populations. *Chaos: An Interdisciplinary Journal of Nonlinear Science*, 22(3):037102, 2012.

[30] Zoltan Neufeld. Stirring effects in models of oceanic plankton populations. *Chaos: An Interdisciplinary Journal of Nonlinear Science*, 22(3):037102, 2012.

[31] Zoltán Neufeld, István Z Kiss, Changsong Zhou, and Jürgen Kurths. Synchronization and oscillator death in oscillatory media with stirring. *arXiv preprint nlin/0307024*, 2003.

[32] Raymond T Pierrehumbert. Lattice models of advection-diffusion. *Chaos: An Interdisciplinary Journal of Nonlinear Science*, 10(1):61–74, 2000.

[33] RT Pierrehumbert. Tracer microstructure in the large-eddy dominated regime. *Chaos, Solitons & Fractals*, 4(6):1091–1110, 1994.

[34] Mathias Sandulescu, Cristóbal López, Emilio Hernández-García, and Ulrike Feudel. Plankton blooms in vortices: the role of biological and hydrodynamic timescales. *Nonlinear Processes in Geophysics*, 14(4), 2007.

[35] HU Sverdrup. On conditions for the vernal blooming of phytoplankton. *Journal du Conseil*, 18(3):287–295, 1953.

[36] John R Taylor and Raffaele Ferrari. Shutdown of turbulent convection as a new criterion for the onset of spring phytoplankton blooms. *Limnology and Oceanography*, 56(6):2293–2307, 2011.

[37] Tamás Tél, Alessandro de Moura, Celso Grebogi, and György Károlyi. Chemical and biological activity in open flows: a dynamical system approach. *Physics reports*, 413(2):91–196, 2005.

[38] Yue-Kin Tsang. Predicting the evolution of fast chemical reactions in chaotic flows. *Physical Review E*, 80(2):026305, 2009.

[39] A Tzella, PH Haynes, et al. Small-scale spatial structure in plankton distributions. *Biogeosciences*, 4(2):173–179, 2007.

[40] Julia Uitz, Hervé Claustre, André Morel, and Stanford B Hooker. Vertical distribution of phytoplankton communities in open ocean: An assessment based on surface chlorophyll. *Journal of Geophysical Research: Oceans (1978–2012)*, 111(C8), 2006.